On the Electrophilicity of Hydroxyl Radical: A Laser Flash Photolysis and Computational Study

ARTICLE *in* JOURNAL OF THE AMERICAN CHEMICAL SOCIETY · JUNE 2005

Impact Factor: 12.11 · DOI: 10.1021/ja043692q · Source: PubMed

J|A|C|S
ARTICLES
Published on Web 04/22/2005

On the Electrophilicity of Hydroxyl Radical: A Laser Flash Photolysis and Computational Study

Matthew P. DeMatteo, James S. Poole,† Xiaofeng Shi, Rakesh Sachdeva, Patrick G. Hatcher, Christopher M. Hadad,* and Matthew S. Platz*

Contribution from the Department of Chemistry, The Ohio State University, 100 West 18th Avenue, Columbus, Ohio 43210

Received October 17, 2004; E-mail: hadad.1@osu.edu; platz.1@osu.edu

Abstract: The rate coefficients for reactions of hydroxyl radical with aromatic hydrocarbons were measured in acetonitrile using a novel laser flash photolysis method. Comparison of kinetic data obtained in acetonitrile with those obtained in aqueous solution demonstrates an unexpected solvent effect on the reactivity of hydroxyl radical. In particular, reactions of hydroxyl radical with benzene were faster in water than in acetonitrile, and by a significant factor of 65. Computational studies, at the B3LYP and CBS-QB3 levels, have confirmed the rate enhancement of hydroxyl radical addition to benzene via calculation of the transition states in the presence of explicit solvent molecules as well as a continuum dielectric field. The origin of the rate enhancement lies entirely in the structures of the transition states and not in the pre-reactive complexes. The calculations reveal that the hydroxyl radical moiety becomes more anionic in the transition state and, therefore, looks more like hydroxide anion. In the transition states, solvation of the incipient hydroxide anion is more effective with water than with acetonitrile and provides the strong energetic advantage for a polar solvent capable of hydrogen bonding. At the same time, the aromatic unit looks more like the radical cation in the transition state. The commonly held view that hydroxyl radical is electrophilic in its reactions with DNA bases is, therefore, strongly dependent on the ability of the organic substrate to stabilize the resulting radical cation.

Introduction

The hydroxyl radical (HO•) is an important member of the diverse class of compounds known collectively as reactive oxygen species (ROS),[1] and these reactive intermediates are involved in a range of biological[2] and environmental[3] processes. Hydroxyl radical is well implicated in DNA damage due to ionizing radiation,[4] and such damage can lead to mutations as well as cell death. Hydroxyl radical, especially in its reactions with DNA,[5] is often categorized as being electrophilic[6] in character; however, other kinetic correlations[7] with nonaromatic organic substrates suggest that hydroxyl radical may not always be electrophilic in its radical addition reactions.

Due to its importance in atmospheric, combustion, and biological and geomedia transformations of organic substrates, hydroxyl radical has been well studied using both experimental and computational methods.[8] We, in particular, have been very interested in understanding the oxidative pathways of hydroxyl radical,[9] as well as other reactive oxygen species,[10] with organic substrates and especially aromatic hydrocarbons.[11]

† Current Address: Department of Chemistry, Ball State University, Muncie, Indiana 47306.

(1) (a) Halliwell, B.; Gutteridge, J. M. C. Oxidative Stress: Adaptation, Damage and Death. In *Free Radicals in Biology and Medicine*; Oxford University Press: Oxford, 1999; pp 246−350. (b) Roberfroid, M.; Calderon, P. B. *Free Radicals and Oxidation Phenomena in Biological Systems*; Marcel Dekker: New York, 1995.

(2) (a) Zweier, J. L.; Villamena, F. V. Chemistry of Free Radicals in Biological Systems. In *Oxidative Stress and Cardiac Failure*; Kukin, M. L., Fuster, V., Eds.; Futura Publishing Co.: Armonk, NY, 2003; pp 67−95. (b) Stadtman, E. R. *Science* **1992**, *257*, 1220−1224. (c) Malins, D. C.; Polissar, N. L.; Gunselman, S. J. *Proc. Natl. Acad. Sci. U.S.A.* **1996**, *93*, 2557−2563.

(3) (a) Blough, N. V.; Zepp, Richard, G. Reactive Oxygen Species in Natural Waters. In *Active Oxygen in Chemistry*; Foote, C. S., Valentine, J. S., Greenberg, A., Liebman, J. F., Eds.; Blackie Academic and Professional: New York, 1995; Vol. 2, pp 280−333. (b) Cooper, W. J.; Curry, R. D.; O'Shea, K. E. *Environmental Applications of Ionizing Radiation*; John Wiley & Sons: New York, 1998.

(4) (a) von Sonntag, C. *The Chemical Basis of Radiation Biology*; Taylor and Francis, Ltd.: London, 1987. (b) Schwarz, H. A. *J. Chem. Educ.* **1981**, *58*, 101−105.

(5) (a) Cadet, J.; Bellon, S.; Berger, M.; Bourdat, A.-G.; Douki, T.; Duarte, V.; Frelon, S.; Gasparutto, D.; Muller, E.; Ravanat, J.-L.; Sauvaigo, S. *Biol. Chem.* **2002**, *383*, 933−943. (b) Breen, A. P.; Murphy, J. A. *Free Radical Biol. Med.* **1995**, *18*, 1033−1077. (c) Cadet, J.; Berger, M.; Douki, T.; Ravanat, J. L. *Rev. Physiol. Biochem. Pharmacol.* **1997**, *131*, 1−87. (d) Burrows, C. J.; Muller, J. G. *Chem. Rev.* **1998**, *98*, 1109−1151. (e) Marnett, L. J. *Carcinogenesis* **2000**, *21*, 361−370. (f) Ames, B. N.; Shigenaga, M. K.; Hagen, T. M. *Proc. Natl. Acad. Sci. U.S.A.* **1993**, *90*, 7915.

(6) (a) Minisci, F.; Galli, R. *Tetrahedron Lett.* **1962**, 533−538. (b) Norman, R. O. C.; Radda, G. K. *Proc. Chem. Soc.* **1962**, 138. (c) Cadet, J.; Douki, T.; Gasparutto, D.; Ravanat, J.-L. *Mutat. Res.* **2003**, *531*, 5−23.

(7) Villamena, F. A.; Hadad, C. M.; Zweier, J. L. *J. Am. Chem. Soc.* **2004**, *126*, 1816−1829.

(8) See for instance, (a) the excellent review by Atkinson, R. *Atmos. Environ., Part A* **1990**, *24A*, 1−41 and the chapters in (i) *Active Oxygen in Chemistry*; Foote, C. S., Valentine, J. S., Greenberg, A., Liebman, J. F., Eds.; Blackie Academic and Professional: New York, 1995; Vol. 2 and (ii) *Active Oxygen in Biochemistry*; Valentine, J. S., Foote, C. S., Greenberg, A., Liebman, J. F., Eds.; Blackie Academic and Professional: New York, 1995; Vol. 3. (b) Volkert, O.; Schulte-Frohlinde, D. *Tetrahedron Lett.* **1968**, 2151−2154. (c) Ashton, L.; Buxton, G. V.; Stuart, C. R. *J. Chem. Soc., Faraday Trans.* **1995**, *91*, 1631−1633. (d) Molina, M. J.; Zhang, R.; Broekhuizen, K.; Lei, W.; Navarro, R.; Molina, L. T. *J. Am. Chem. Soc.* **1999**, *121*, 10225−10226. (e) Volkamer, R.; Klotz, B.; Barnes, I.; Imamura, T.; Wirtz, K.; Washida, N.; Becker, K. H.; Platt, U. *Phys. Chem. Chem. Phys.* **2002**, *4*, 1598−1610.

(9) (a) Villamena, F. A.; Hadad, C. M.; Zweier, J. L. *J. Phys. Chem. A* **2003**, *107*, 4407−4414. (b) Villamena, F. A.; Gallucci, J.; Velayutham, M.; Hadad, C. M.; Zweier, J. L. *J. Org. Chem.* **2004**, *69*, 7994−8004.

10.1021/ja043692q CCC: $30.25

Of particular interest to environmental chemists is the observation that hydroxyl radical, and other reactive intermediates, may be generated photochemically from dissolved humic materials in water,[12] and these species may assist in the decomposition of persistent environmental pollutants, such as polycyclic aromatic hydrocarbons (PAHs).

Experimentally, the kinetics of hydroxyl radical in aqueous solution have been studied for a wide range of organic and inorganic molecules, largely by a combination of pulse radiolysis[13] and laser flash photolysis[14] (LFP) methods. Much of the data obtained has been collated and published.[15] However, studies of the kinetics of reaction of hydroxyl radical with PAHs in aqueous solution are hampered by the poor solubility of these compounds in water. Moreover, there is an increasing body of evidence to suggest that such compounds form associative interactions with humic materials, and thus the environment in which hydroxyl radical and PAHs interact in nature may not be truly aqueous in nature.[16]

We have developed an LFP-based experimental methodology that allows us to measure the rate of reaction for hydroxyl radical with aromatic compounds in acetonitrile, a polar, non-hydroxylic solvent with relatively low reactivity toward hydroxyl radical.[15] In this contribution, the rate coefficients for the reaction of hydroxyl radical with benzene and naphthalene in acetonitrile were determined and compared with the data obtained in aqueous solution. Computational studies were then used to rationalize the unexpected experimental results and to discover the origin of this effect.

Experimental and Computational Methods

The LFP system used at the Ohio State University has been described in detail previously.[17] HPLC grade acetonitrile and benzene were obtained from commercial sources and distilled over CaH_2 prior to use. Naphthalene, *trans*-stilbene and *N*-hydroxypyridine-2-thione (**1**) were obtained from commercial sources and used as received.

Solutions (2 mL) consisting of *N*-hydroxypyridin-2-thione (5×10^{-4} M), *trans*-stilbene (held constant between 0.010 and 0.015 M), and the aromatic competitors benzene, benzene-d_6, and naphthalene (serial concentrations between 0 and 1.10 M, depending on the reactivity of the competitor) were deoxygenated using a thin stream of bubbling argon. The concentrations of *N*-hydroxypyridin-2-thione (PSH) and *trans*-stilbene were chosen to provide optimal signal intensity from the system (an overall optical density for PSH of about 1.8−2.0 at 355 nm). Solutions were photolyzed at 355 nm (third harmonic of Nd:YAG laser, nominal pulse width = 10 ns), and the transient absorbance signal was monitored at 392 nm.

Quantitative gas chromatographic (GC) studies were performed on a Hewlett-Packard 6890 system fitted with an automatic injector and a flame ionization detector. The column used for the GC-FID was an Rtx-5 column with 5% diphenyl/95% dimethyl polysiloxane stationary phase (length: 30 M, diameter: 0.25 mm, film thickness: 0.25 μM) manufactured by Restek. The GC conditions were the following: initial temperature of 60 °C, hold for 2 min; increase of 25 °C/min to 100 °C, hold for 8 min; increase of 25 °C/min to 250 °C, hold for 10 min; along with an inlet temperature of 280 °C and a detector temperature of 300 °C. GC−MS measurements were performed with a Hewlett-Packard 6890 GC system with a 5973 mass selective detector. The column used for GC−MS was an HP-5MS column with parameters identical to those of the Rtx-5. Typically, six solutions with three different ratios of benzene to naphthalene (4.7:1, 14.1:1, and 42.3:1) were photolyzed in acetonitrile in the presence of 10 mM *N*-hydroxypyridine-2-thione (**1**) at 365 nm for 12 to 15 h in a Ray-O-Net reactor. The solutions were degassed with argon before photolysis. The resulting solution was derivatized with an equivalent volume of BSTFA (bis-(trimethylsilyl)trifluoroacetamide) from Supelco. The solutions were then analyzed by GC-FID, and the chromatographs were integrated using the area normalization technique to determine the relative ratios of phenol and naphthol derivatives. A series of phenol/1-naphthol solutions with known concentrations were derivatized and analyzed by GC-FID to obtain the response of the ratio of signal intensity vs concentration of authentic phenol and naphthol. The retention times of phenol (6.66 min) and 1-naphthol (16.13 min) derivatives were obtained directly by standards on GC-FID, while that of 2-naphthol (16.27 min) was determined based on the GC−MS chromatogram.

All calculations, unless otherwise specified, were performed with Gaussian 98.[18] To probe the complexes formed between hydroxyl radical and solvent, a variety of possible complexes were first optimized using density functional theory (DFT) at the B3LYP/6-31+G** level of theory.[19] Two different complexes of hydroxyl radical and a single solvent molecule were located in each solvent (two with acetonitrile and two with water). Single-point energy calculations were then performed at the B3LYP/6-311+G** level of theory with six Cartesian d functions. Further analysis was performed by optimizing these geometries at the MP2/6-3l+G** level of theory.[20] Single-point energy calculations were performed with the resulting geometries at the MP2/6-311+G** level of theory with six Cartesian d functions. One of the complexes was a transition state at the B3LYP level, and a corresponding structure at the MP2 level could not be located. Therefore, at the MP2 level, only two complexes of hydroxyl radical with water and one complex with acetonitrile were found.

(10) Villamena, F. A.; Merle, J. K.; Hadad, C. M.; Zweier, J. L. *J. Phys. Chem. A*, submitted.
(11) (a) Barckholtz, C.; Barckholtz, T. A.; Hadad, C. M. *J. Am. Chem. Soc.* **1999**, *121*, 491−500. (b) Barckholtz, C.; Fadden, M. J.; Hadad, C. M. *J. Phys. Chem. A* **1999**, *103*, 8108−8117. (c) Fadden, M. J.; Barckholtz, C.; Hadad, C. M. *J. Phys. Chem. A* **2000**, *104*, 3004−3011. (d) Fadden, M. J.; Hadad, C. M. *J. Phys. Chem. A* **2000**, *104*, 6088−6094. (e) Fadden, M. J.; Hadad, C. M. *J. Phys. Chem. A* **2000**, *104*, 6324−6331. (f) Barckholtz, C.; Barckholtz, T. A.; Hadad, C. M. *J. Phys. Chem. A* **2001**, *105*, 140−152. (g) Briggs, M. K.; Desavis, E.; Mazzer, P. A.; Sunoj, R. B.; Hatcher, S. A.; Hadad, C. M.; Hatcher, P. G. *Chem. Res. Toxicol.* **2003**, *16*, 1484−1492. (h) Onchoke, K. K.; Hadad, C. M.; Dutta, P. K. *Polycyclic Aromat. Cmpd.* **2004**, *24*, 37−64.
(12) Vaughan, P. P.; Blough, N. V. *Environ. Sci. Technol.* **1998**, *32*, 2947.
(13) Baxendale, J. H.; Rodgers, M. A. J. *Chem. Soc. Rev.* **1978**, *7*, 235−163. (b) Adams, G. E.; Wardman, P. *Free Radicals Biol.* **1977**, *3*, 53−95.
(14) Scaiano, J. C. Nanosecond Laser Flash Photolysis: A Tool for Physical Organic Chemistry. In *Reactive Intermediate Chemistry*; Moss, R. A., Platz, M. S., Jones, M., Jr., Eds.; John Wiley & Sons: Hoboken, NJ, 2004; pp 797−845.
(15) A large amount of experimental data has been compiled by the University of Notre Dame's Radiation Laboratory, supported by the U.S. Department of Energy and in conjunction with the National Institute of Science and Technology: http://www.rcdc.nd.edu/compilations/Hydroxyl/OH.htm.
(16) (a) Salloum, M.; Chefetz, B.; Hatcher, P. G. *Environ. Sci. Technol.* **2002**, *36*, 1953. (b) Chefetz, B.; Deshmukh, A. P.; Hatcher, P. G.; Guthrie, E. A. *Environ. Sci. Technol.* **2000**, *34*, 2925.
(17) (a) Martin, C. B.; Shi, X.; Tsao, M.-L.; Karwiek, D.; Brooke, J.; Hadad, C. M.; Platz, M. S. *J. Phys. Chem. B* **2002**, *106*, 10263. (b) Gritsan, N. P.; Zhai, H. B.; Yuzawa, T.; Karweik, D.; Brooke, J.; Platz, M. S. *J. Phys. Chem. A* **1997**, *101*, 2833.
(18) Frisch, M. J.; Trucks, G. W.; Schlegel, H. B.; Scuseria, G. E.; Robb, M. A.; Cheeseman, J. R.; Zakrzewski, V. G.; Montgomery, J. A., Jr.; Stratmann, R. E.; Burant, J. C.; Dapprich, S.; Millam, J. M.; Daniels, A. D.; Kudin, K. N.; Strain, M. C.; Farkas, O.; Tomasi, J.; Barone, V.; Cossi, M.; Cammi, R.; Mennucci, B.; Pomelli, C.; Adamo, C.; Clifford, S.; Ochterski, J.; Petersson, G. A.; Ayala, P. Y.; Cui, Q.; Morokuma, K.; Malick, D. K.; Rabuck, A. D.; Raghavachari, K.; Foresman, J. B.; Cioslowski, J.; Ortiz, J. V.; Stefanov, B. B.; Liu, G.; Liashenko, A.; Piskorz, P.; Komaromi, I.; Gomperts, R.; Martin, R. L.; Fox, D. J.; Keith, T.; Al-Laham, M. A.; Peng, C. Y.; Nanayakkara, A.; Gonzalez, C.; Challacombe, M.; Gill, P. M. W.; Johnson, B.; Chen, W.; Wong, M. W.; Andres, J. L.; Gonzalez, C.; Head-Gordon, M.; Replogle, E. S.; Pople, J. A. *Gaussian 98*, Revision A.7; Gaussian, Inc.: Pittsburgh, PA, 1998.
(19) (a) Labanowski, J. W.; Andzelm, J. *Density Functional Methods in Chemistry*; Springer: New York, 1991. (b) Parr, R. G.; Yang, W. *Density Functional Theory in Atoms and Molecules*; Oxford University Press: New York, 1989. (c) Becke, A. D. *J. Chem. Phys.* **1993**, *98*, 5648. (d) Lee, C.; Yang, W.; Parr, R. G. *Phys. Rev. B* **1988**, *37*, 785.
(20) (a) Moller, C.; Plesset, M. S. *Phys. Rev.* **1934**, *46*, 618−622. (b) Hehre, W. J.; Radom, L.; Schleyer, P. v. R.; Pople, J. A. *Ab Initio Molecular Orbital Theory*; Wiley-Interscience: New York, 1986. (c) Pople, J. A.; Binkley, J. S.; Seger, R. *Int. J. Quantum Chem. Symp.* **1976**, *10*, 1.

The stationary points on the potential energy surface of the radical addition and hydrogen-atom abstraction reactions with benzene were then analyzed using density functional theory. Transition states for each process were located at the B3LYP/6-31+G** level of theory. Calculation of the vibrational frequencies confirmed these optimized structures to be transition states. To locate the reactants and products connected by these transition states, the transition-state geometries were displaced by 10% along the normal coordinate for the imaginary vibrational frequency and then optimized with the analytical second derivatives (opt = calcfc). Single-point energy calculations were performed on each stationary point at the B3LYP/6-311+G** level of theory with six Cartesian d functions. To explore the effect of the dielectric constants of water and acetonitrile on the hydroxyl radical addition reaction, the transition states were optimized with the polarizable continuum model (PCM)[21] B3LYP/6-31+G** level of theory for each of the solvents, and single-point energies were obtained at the PCM B3LYP/6-311+G** level using those optimized geometries. These PCM calculations were performed with the Gaussian 03 software package.[22] Reactants and products were located in the same manner as described above.

The same process described above was also used to locate the gas-phase transition states, reactants and products for the reaction of complexes of hydroxyl radical, and one explicit solvent molecule (either water or acetonitrile) with benzene at the B3LYP/6-31+G** level. The B3LYP transition-state geometries were also obtained at the CBS-QB3 level of theory.[23] Vibrational frequency analysis confirmed the optimized geometries to be transition states, i.e., each stationary point possessed only one imaginary vibrational frequency. By displacement along the reaction coordinate, as above, the reactants and products were located for the reactions. Second-order rate constants were calculated for these reactions according to the following equation:

$$\text{rate}\ (\text{s}^{-1}) = \frac{k_\text{B}T}{h}\, \text{e}^{-\Delta G^{\ddagger}/RT}$$

A Wigner tunneling correction[24] was applied to these rates according to the equation:

$$1 + \left(\frac{1}{24}\right)\left[\frac{h\omega}{2\pi k_\text{B}T}\right]^2$$

in which ω is the imaginary vibrational frequency for the transition state.

To explore the effect of the dielectric field of the solvent on the reaction of hydroxyl radical complexed with one explicit solvent molecule, single-point energy calculations were performed on the B3LYP geometries for the complexes using the polarizable continuum model (PCM).[21] Single-point energies were calculated at the PCM B3LYP/6-311+G** level of theory with either water or acetonitrile as the solvent.

Scheme 1. Photolytic Decomposition of *N*-Hydroxypyridin-2-thione

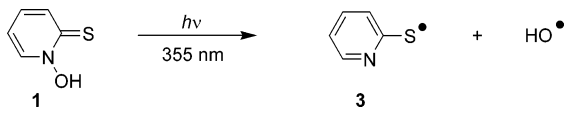

1 **3**

Natural population analysis (NPA)[25] methods were used for each of the stationary points to determine the charge and spin density on each atom of the systems. The calculations were performed for the single-point energy calculations at the B3LYP/6-311+G** level of theory using the B3LYP/6-31+G** geometries.

To determine the effect of multiple solvent molecules in the reaction of hydroxyl radical with benzene, a Monte Carlo search was performed using the Monte Carlo multiple minimum (MCMM) search protocol as implemented in MacroModel version 8.5.[26] Energy minimizations were performed with the MM3 force field. The conformational search was performed using two different systems. The first system involved 5-hydroxy-1,3-cyclohexadiene (**2**) and two molecules of solvent (either water or acetonitrile). The second system involved structure **2** and three molecules of solvent. This allowed for the solvent molecules to vary their positions in the systems.

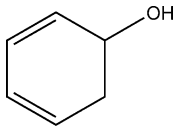

2

The three lowest-energy geometries (at the MM3 level) were selected for each system. The ring in each geometry was planarized, the extraneous hydrogen at C-6 was removed, and the C−O bond length was lengthened to produce a suitable guess for the transition state for the addition of hydroxyl radical to benzene at the B3LYP/6-31+G** level of theory. The result was that only one transition-state geometry for each solvent system was located, but manual rotation about the C−O bond allowed for a second transition state to be located for each system. Reactants and products for each transition state were located in the same manner as described above. Single-point energies were performed at the B3LYP/6-311+G** level of theory. As a final test, a mixed system with one molecule of water and one molecule of acetonitrile forming the complex with hydroxyl radical was analyzed in this same manner. Transition states for the addition to benzene were located, as well as reactants and products.

Results and Discussion

Laser Flash Photolysis. Hydroxyl radical was generated by photolysis of *N*-hydroxypyridine-2-thione (**1**) at 355 nm (generated from a Nd:YAG laser, nominal pulse width = 10 ns) as shown in Scheme 1. The photolysis of this compound has been investigated previously by Aveline et al.,[27] and these workers determined that in nonaqueous solution, compound **1** is photolyzed relatively cleanly to yield hydroxyl radical and the

(21) (a) Miertus, S.; Scrocco, E.; Tomasi, J. *Chem. Phys.* **1981**, *55*, 117. (b) Cammi, R.; Tomasi, J. *J. Comput. Chem.* **1995**, *16*, 1449. (c) Tomasi, J.; Persico, M. *Chem. Rev.* **1994**, *94*, 2027. (d) Cramer, C. J.; Truhlar, D. J. *Chem. Rev.* **1999**, *99*, 2161.
(22) Frisch, M. J.; Trucks, G. W.; Schlegel, H. B.; Scuseria, G. E.; Robb, M. A.; Cheeseman, J. R.; Montgomery, J. A., Jr.; Vreven, T.; Kudin, K. N.; Burant, J. C.; Millam, J. M.; Iyengar, S. S.; Tomasi, J.; Barone, V.; Mennucci, B.; Cossi, M.; Scalmani, G.; Rega, N.; Pettersson, G. A.; Nakatsuji, H.; Hada, M.; Ehara, M.; Toyota, K.; Fukuda, R.; Hasegawa, J.; Ishida, M.; Nakajima, T.; Honda, Y.; Kitao, O.; Nakai, H.; Klene, M.; Li, X.; Knox, J. E.; Hratchian, H. P.; Cross, J. B.; Adamo, C.; Jaramillo, J.; Gomperts, R.; Stratmann, R. E.; Yazyev, O.; Austin, A. J.; Cammi, R.; Pomelli, C.; Ochterski, J. W.; Ayala, P. Y.; Morokuma, K.; Voth, G. A.; Salvador, P.; Dannenberg, J. J.; Zakrzewski, V. G.; Dapprich, S.; Daniels, A. D.; Strain, M. C.; Farkas, O.; Malick, D. K.; Rabuck, A. D.; Raghavachari, K.; Foresman, J. B.; Ortiz, J. V.; Cui, Q.; Baboul, A. G.; Clifford, S.; Cioslowski, J.; Stefanov, B. B.; Lui, G.; Liashenko, A.; Piskorz, P.; Komaromi, I.; Martin, R. L.; Fox, D. J.; Keith, T.; Al-Laham, M. A.; Peng, C. Y.; Nanayakkara, A.; Challacombe, M.; Gill, P. M. W.; Johnson, B.; Chen, W.; Wong, M. W.; Gonzalez, C.; Pople, J. A. *Gaussian 03*, Revision B.04; Gaussian, Inc.: Pittsburgh, PA, 2003.
(23) Montgomery, J. A., Jr.; Frisch, M. J.; Ochterski, J. W.; Petersson, G. A. *J. Chem. Phys.* **1999**, *110*, 2822−2827.
(24) Wigner, E. P. *Phys. Rev.* **1955**, *98*, 145.
(25) (a) Reed, A. E.; Weinstock, R. B.; Weinhold, F. *J. Chem. Phys.* **1985**, *83*, 735. (b) Reed, A. E.; Weinhold, F.; Curtiss, J. A. *Chem. Rev.* **1988**, *88*, 899.
(26) Mohamadi, F.; Richards, N. G. J.; Guida, W. C.; Liskamp, R.; Lipton, M.; Caulfield, C.; Chang, G.; Hendrickson, T.; Still, W. C. *J. Comput. Chem.* **1990**, *11*, 440. (b) Goodman, J.; Still, W. C. *J. Comput. Chem.* **1991**, *12*, 1110.
(27) (a) Aveline, B. M.; Kochevar, I. E.; Redmond, R. W. *J. Am. Chem. Soc.* **1996**, *118*, 10124. (b) Aveline, B. M.; Kochevar, I. E.; Redmond, R. W. *J. Am. Chem. Soc.* **1996**, *118*, 10113.

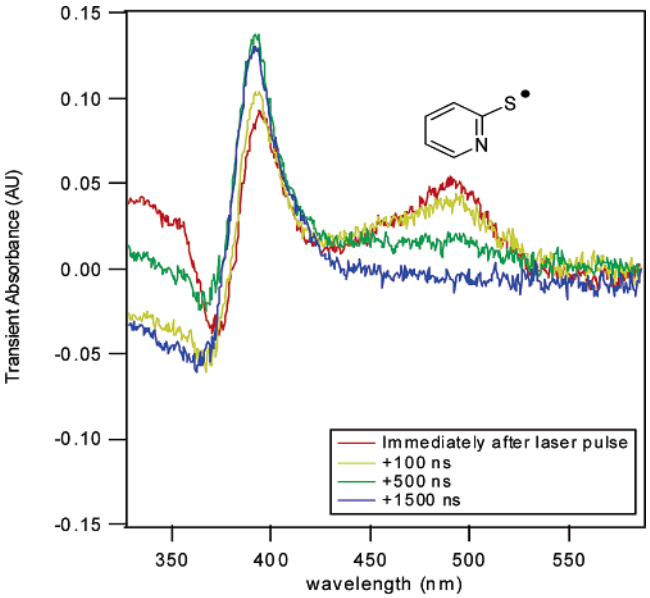

Figure 1. Transient absorbance spectra obtained following laser flash photolysis of an acetonitrile solution of 0.65 mM **1** (PSH) with 355 nm light in the presence of 15 mM *trans*-stilbene. The broad feature at 470 nm corresponds to the transient absorption spectrum of thiyl radical **3**.

pyrithiyl radical (**3**) (Scheme 1). The intermediate **3** has a broad transient absorbance in the visible region with a maximum at 490 nm (Figure 1). Unfortunately, hydroxyl radical does not have a diagnostic UV−vis absorption at convenient wavelengths (300−700 nm) in solution-phase LFP experiments. Thus, we have utilized *trans*-stilbene as a probe molecule which generates a useful and convenient UV−vis signature of the adduct of hydroxyl radical with *trans*-stilbene. The kinetics of formation of the adduct are equal to the kinetics of hydroxyl radical decay and can be used to obtain the absolute reaction rate constants of the "invisible" radical of interest following methodology pioneered by Scaiano for other radicals.[14]

LFP of **1** in the presence of *trans*-stilbene generates an absorbance signal at 392 nm in acetonitrile (Figure 1). Analysis of this signal indicates that it is the sum of two chemical processes: one process involves a reactive intermediate which is both rapidly formed and consumed on the nanosecond time scale (Figure 2). The other process involves an intermediate which is formed and is persistent on the microsecond time scale (Figure 3). The second process was observed in the absence of *trans*-stilbene, and originally by Aveline et al.[27] who attributed the signal to secondary reactions of **3** which generated closed-shell species. It is likely that the reaction is the dimerization of two units of the pyrithiyl radical (**3**) to form the resulting disulfide.

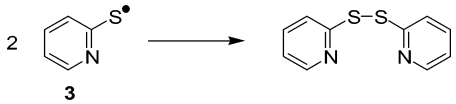

3

Alternatively, the nanosecond signal may be due to secondary reactions of cyanomethyl radical (formed by rapid (10 ns) reaction of hydroxyl radical with the solvent) with *trans*-stilbene. The rapidly growing signal observed on the nanosecond time scale in the presence of *trans*-stilbene can be fit to an exponential

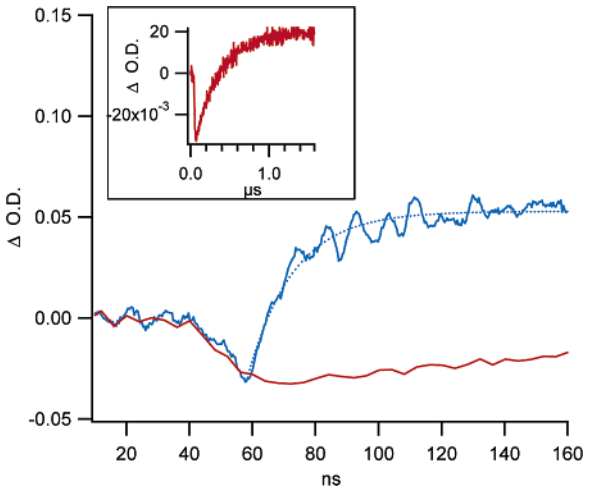

Figure 2. Decay curves measured at 392 nm following photolysis of 0.65 mM **1** in the presence (blue) and absence (red) of 15 mM *trans*-stilbene for the first 160 ns. The inset shows the transient absorption spectrum after photolysis (355 nm) of **1** at longer time scales in the absence of *trans*-stilbene.

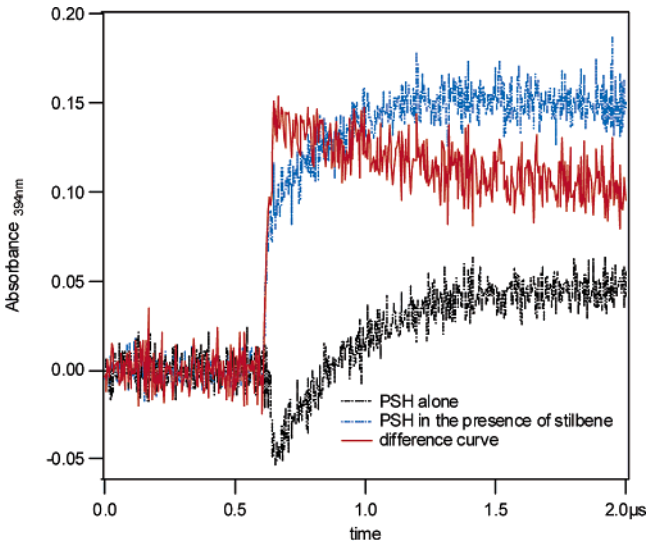

Figure 3. Decay curves measured at 392 nm following photolysis of 0.65 mM **1** in the presence (blue) and absence (black) of 15 mM *trans*-stilbene. The red curve is a difference curve, showing the rapid formation and decay of the intermediate generated by reaction of hydroxyl radical with *trans*-stilbene.

function to yield an observed pseudo-first-order rate constant, k_{obs}. Under the experimental conditions

$$k_{obs} = \frac{1}{\tau} + k\,[\textit{trans}\text{-stilbene}]$$

where τ is the lifetime of the short-lived reactive intermediate (which reacts with *trans*-stilbene) in the absence of *trans*-stilbene and k is the second-order rate constant for reaction of that reactive intermediate with *trans*-stilbene. Thus, plots of k_{obs} versus *trans*-stilbene concentration should be linear. In fact, the observed pseudo-first-order rate constant for formation of the transient absorption (k_{obs}) measured at short time scales is linearly dependent on the concentration of *trans*-stilbene (Figure 4). A plot of the dependence of the measured fast growth rate constant vs the concentration of *trans*-stilbene provides the absolute second-order rate constant for reaction of a transient

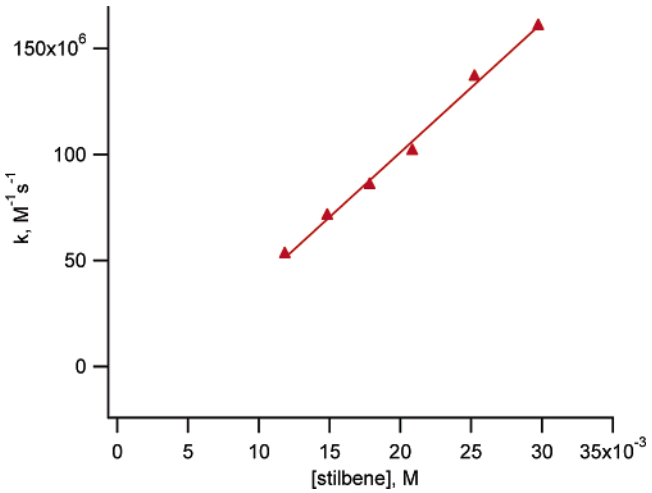

Figure 4. Observed pseudo-first-order rate constant for the growth of transient absorbance at 392 nm following laser flash photolysis of **1** in acetonitrile as a function of the concentration of *trans*-stilbene. The slope (6.1×10^9) of the plot gives the total absolute second-order rate constant for reaction of hydroxyl radical with *trans*-stilbene which includes all hydrogen-atom abstraction and radical-addition processes. (The intercept of the plot is -2.0×10^7.)

species with *trans*-stilbene in acetonitrile of $(6.1 \pm 0.2) \times 10^9$ M^{-1} s^{-1} at ambient temperature.

This 355-nm LFP experiment was repeated with the hydroxyl-radical precursor (PSH, **1**) in CCl_4 as a function of *trans*-stilbene concentration (see Supporting Information). In CCl_4, a species is generated which reacts with *trans*-stilbene with a rate constant of 9×10^9 M^{-1} s^{-1}, and with a lifetime of $\sim$1 μs in the absence of *trans*-stilbene. Therefore, the species which reacts with *trans*-stilbene has roughly the same reactivity and lifetime in CCl_4 and CH_3CN. Thus, it is unlikely that we are probing the reactivity of a solvent-derived radical, and the most economical explanation of these data is that the LFP experiments are directly probing the generation and reactivity of hydroxyl radical with *trans*-stilbene.

Figure 4 provides the absolute rate constant for reaction of hydroxyl radical with *trans*-stilbene (via all modes of reaction) of $(6.1 \pm 0.2) \times 10^9$ M^{-1} s^{-1} in acetonitrile at 298 K. The intercept of this curve provides an estimate of the lifetime of hydroxyl radical in the presence of all other species in this system, including acetonitrile, in the absence of *trans*-stilbene. The measured lifetime was 50 ns. This provides an upper limit for the rate constant for reaction of hydroxyl radical with acetonitrile of 1.0×10^6 M^{-1} s^{-1}, assuming that neat acetonitrile has a concentration of 19.17 M at 298 K. This rate constant is approximately a factor of 20 smaller than the value measured for the same reaction in aqueous solution.[28] This observation is consistent with subsequent observations made in conjunction with the reaction of hydroxyl radical with aromatic hydrocarbons, both in qualitative behavior and in magnitude, which are discussed below.

There are a number of potential sites on *trans*-stilbene where hydroxyl radical may attack, and DFT calculations were performed to determine which of the potential intermediates (Scheme 2) was responsible for the observed transient absorbance. The calculations were performed on intermediates arising from hydroxyl radical addition, rather than H-atom abstraction, as a first approximation. The structure of each potential intermediate was optimized at the B3LYP/6-31G* level of theory, and the absorbance spectrum for each was estimated by calculating the gas-phase vertical transitions for each potential intermediate using time-dependent density functional theory (TD B3LYP/6-31+G**//B3LYP/6-31G* level).[29] The results obtained are summarized in Table 1. The heats of reaction for the radical adducts were determined relative to the combined energies for infinitely separated *trans*-stilbene and hydroxyl radical. The second-order rate constant of reaction measured by LFP is the sum of all rate constants of all processes by which hydroxyl radical reacts with *trans*-stilbene.

The results indicate that hydroxyl-radical addition to *trans*-stilbene is a thermodynamically favorable process, with addition to the olefin double bond yielding the most thermodynamically stable addition adduct. However, this species appears to have no strong absorbance near the experimentally observed signal at 392 nm; however, there is a small (but very weak) absorption predicted at 380 nm for the alkene adduct. Addition of hydroxyl radical *ortho*- and *para*- to the double bond yields intermediates that do exhibit the requisite absorption characteristics. Addition of hydroxyl radical at the *meta*- and *ipso*- positions are less favorable and do not generate intermediates with the appropriate absorbance characteristics. Therefore, we conclude that our observed transient absorption is predominantly due to a combination of *ortho*- and *para*- substituted hydroxyl radical adducts.

With this information in hand, we have used this LFP method to measure the kinetics of hydroxyl radical with benzene and naphthalene, molecules we may consider to be models for larger PAHs. The rate coefficient for reaction of hydroxyl radical with benzene was measured in two ways: by measuring the dependence of the fast pseudo-first-order growth rate constant with the concentration of benzene (Figure 5), and by measuring the dependence of the maximum transient absorbance intensity with the concentration of benzene (Stern−Volmer competitive kinetic analysis, Figure 6). Under these conditions:

$$k_{obs} = \frac{1}{\tau} + k\,[\textit{trans}\text{-stilbene}] + k'\,[\text{benzene}]$$

where k' is the absolute second-order rate constant for reaction of hydroxyl radical with benzene. Thus, the slope of Figure 5 yields the rate constant of interest k' for hydroxyl radical reaction with benzene.

The behavior of the transient intermediates on the microsecond time scale is shown in Figure 3. The Stern−Volmer analysis was performed by subtracting the slow-growing signal observed in the absence of *trans*-stilbene from the rapidly formed, slowly decaying signal observed in the presence of *trans*-stilbene (and in some cases, *trans*-stilbene plus arene). The maximum transient absorbances (A) at 392 nm, which were present 50−150 ns after the laser pulse, were taken to be the values of $A_{0,392}$ (*trans*-stilbene only) and A_{392} (*trans*-stilbene plus arene) in the Stern−Volmer analysis (Figure 6). In Figure 5, the background signal (zero *trans*-stilbene) was not subtracted from the signal obtained in the presence of *trans*-stilbene and arene.

(28) Neta, P.; Schuler, R. H. *J. Phys. Chem.* **1975**, *79*, 1−6.
(29) TD-DFT has been used successfully to simulate electronic spectra (vertical transitions) of organic molecules. For example, see (a) Wiberg, K. B.; Stratmann, R. E.; Frisch, M. J. *Chem. Phys. Lett.* **1998**, *297*, 60. (b) van Gisbergen, S. J. A.; Rosa, A.; Ricciardi, G.; Baerends, E. J. *J. Chem. Phys.* **1999**, *111*, 2499. (c) Poole, J. S.; Hadad, C. M.; Platz, M. S.; Fredin, Z. P.; Pickard, L.; Levya-Guerrero, E.; Kessler, M.; Chowdhury, G.; Kotandenyia, D.; Gates, K. S. *Photochem. Photobiol.* **2002**, *75*, 339.

Scheme 2. Potential Intermediates from the Reaction of Hydroxyl Radical with Stilbene

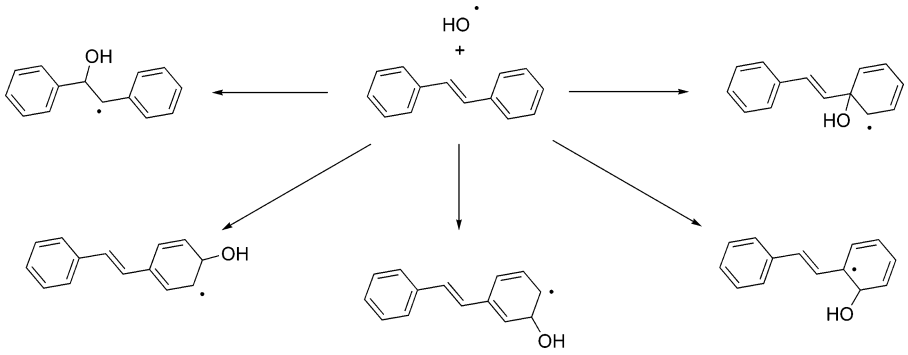

Table 1. Summary of Density Functional Theory and Time-Dependent Density Functional Theory Calculations for All Possible Intermediates Arising from Addition of Hydroxyl Radical to *trans*-Stilbene

	point of hydroxyl radical attack									
	alkene		*ipso-*		*ortho-*		*meta-*		*para-*	
E (hartrees)[a]	−616.49023		−616.45313		−616.46673		−616.45819		−616.47082	
ZPE (hartrees)[b]	0.22973		0.22784		0.22826		0.22789		0.22861	
ΔH_R (kJ/mol)[c]	−136		−43		−77		−55		−87	
vertical transitions[d]	λ (nm)	f[e]	λ (nm)	f[e]	λ (nm)	f[e]	λ (nm)	f[e]	λ (nm)	f[e]
	380	0.012	429	0.016	437	0.402	432	0.015	378	0.260
	305	0.072	387	0.010	421	0.253	305	0.161	370	0.617
			289	0.039	336	0.015	301	0.787	348	0.066
					330	0.021	291	0.013	338	0.018
					316	0.010			335	0.212
									311	0.013

[a] Energy calculated at the B3LYP/6-31G* level, geometry optimized at B3LYP/6-31G* level of theory. [b] Unscaled ZPE as calculated at the B3LYP/6-31G* level, number of imaginary frequencies = 0. [c] Relative enthalpy as calculated at 298 K, relative to the sum of energies for isolated hydroxyl radical and stilbene at the B3LYP/6-31G* level of theory. [d] Calculated by time-dependent DFT at the TD B3LYP/6-311+G**//B3LYP/6-31G* level of theory—only the first 10 spin-allowed transitions were calculated. [e] Oscillator strength for transition. Only transitions with significant calculated oscillator strengths (≥0.01) are included.

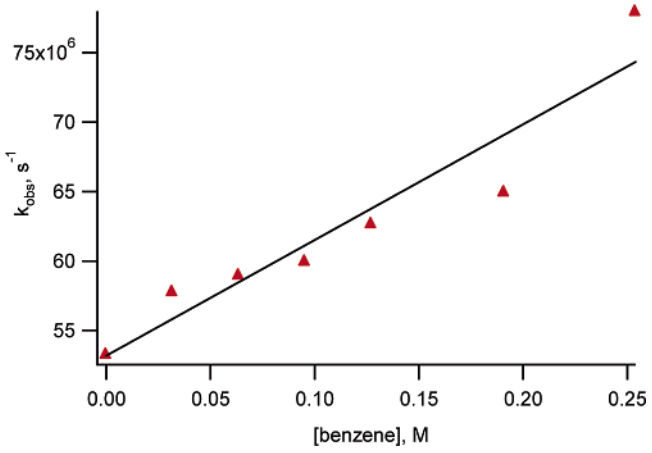

Figure 5. Observed pseudo-first-order rate constant (k_{obs}) for the growth of transient absorbance at 392 nm following laser flash photolysis of **1** in acetonitrile with 12 mM *trans*-stilbene as a function of the concentration of benzene.

The rate coefficients for reaction of hydroxyl radical with benzene-d_6 and naphthalene were determined only by Stern−Volmer kinetic analyses. The Stern−Volmer treatment also yields the ratio of the sum of all rate constants for hydroxyl reaction with the substrate (abstraction of each type of hydrogen and addition to each carbon) relative to the sum of all rate constants for reaction with *trans*-stilbene (abstraction of each type of hydrogen and addition to each carbon). The experimental results are shown in Table 2.

For benzene, the results obtained by both methods are consistent with one another within experimental uncertainty, and the results obtained for benzene and benzene-d_6 yield a kinetic isotope effect (KIE) of 1.0 ± 0.3, indicating that the reaction of hydroxyl radical with this compound is dominated by radical addition, and not abstraction, as expected from the calculations.

Perhaps the most remarkable feature of the data in Table 2 are the absolute second-order rate constants for reaction of hydroxyl radical with these compounds in acetonitrile in comparison with those obtained in aqueous solution.[15,30] Initially, we expected that hydroxyl radical would exhibit lower reactivity in water, since it may form hydrogen bonds with water and form a solvation shell[31]—an option not readily available for a polar, but non-hydroxylic, solvent such as acetonitrile. The data obtained show the exact opposite trend—the rate coefficient for reaction of hydroxyl radical with naphthalene is some 5.8 times slower in acetonitrile than in water, and the rate coefficient for reaction of hydroxyl radical with benzene is some 65 times slower in acetonitrile than in water.

As mentioned previously, the LFP data indicate that the absolute reactivity of hydroxyl radical with aromatic rings is reduced in acetonitrile relative to water. Furthermore, the ratio

(30) (a) Buxton, G. V.; Greenstock, C. L.; Helman, W. P.; Ross, A. B. *J. Phys. Chem. Ref. Data* **1988**, *17*, 513. (b) Dorfman, L. M.; Taub, I. A.; Buehler, R. E. *J. Chem. Phys.* **1962**, *36*, 3051. (c) Roder, M.; Wojnarovits, L.; Foldiak, G. *Radiat. Phys. Chem.* **1990**, *36*, 175.

(31) Water complexes have been observed and characterized by matrix IR. For examples, see: (a) Engdahl, A.; Karlström, G.; Nelander, B. *J. Chem. Phys.* **2003**, *118*, 7797. (b) Langford, V. S.; McKinley, A. J.; Quickenden, T. I. *J. Am. Chem. Soc.* **2000**, *122*, 12859. We note that acetonitrile complexes of hydroxyl radical have not yet been similarly characterized.

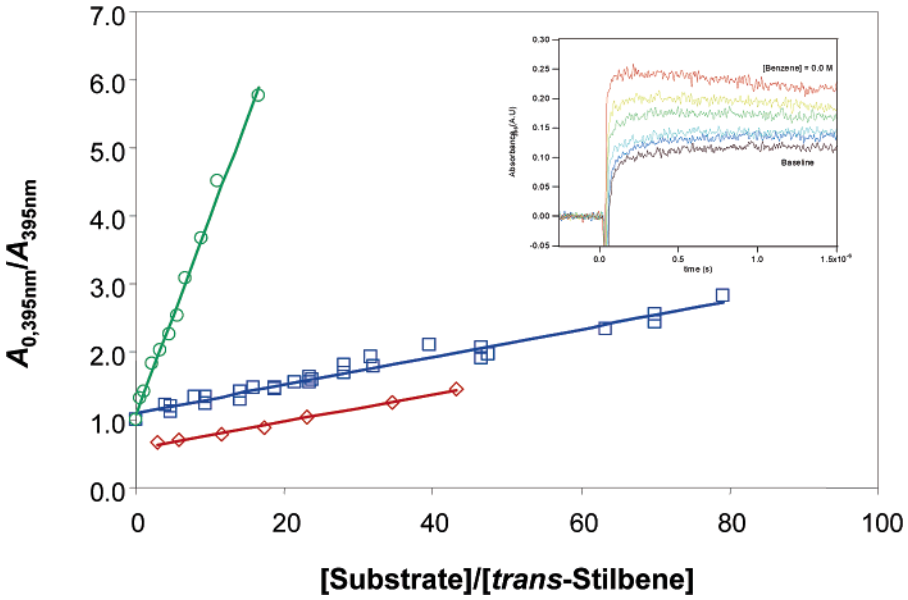

Figure 6. Stern−Volmer plots for benzene (open squares), benzene-d_6 (open diamonds, offset by −0.5 for clarity), and naphthalene (open circles) as a function of the substrate/*trans*-stilbene relative concentration. The derived rate constants for reaction of hydroxyl radical, relative to reaction with *trans*-stilbene [$(6.1 \pm 0.2) \times 10^9$ M^{-1} s^{-1}], were found to be 0.0205 ($R^2 = 0.969$), 0.0198 ($R^2 = 0.993$), and 0.290 ($R^2 = 0.994$), for benzene, benzene-d_6, and naphthalene, respectively. Inset: quenching of transient absorption signal at 392 nm with increasing concentration of benzene. For reasons of clarity, the decay curves have been smoothed.

Table 2. Kinetic Data for Reaction of Hydroxyl Radical with Aromatic Hydrocarbons in Acetonitrile (ACN) and Water (aq)

substrate	method[a]	$k_{substr}/k_{stilbene}$	R^2 [b]	$k_{substr,ACN}$ $(M^{-1}s^{-1})$[c]	$k_{substrate,aq}$ $(M^{-1}s^{-1})$[d]
benzene	direct			$(8.3 \pm 1.2) \times 10^7$	7.8×10^9[e]
	comp	0.0209 ± 0.0012	0.98	$(1.2 \pm 0.1) \times 10^8$	7.8×10^9[e]
benzene-d_6	comp	0.0198		$(1.2 \pm 0.1) \times 10^8$	4.7×10^9[f]
naphthalene	comp	0.290 ± 0.007	1.00	$(1.8 \pm 0.1) \times 10^9$	9.4×10^9[g]

[a] direct = direct measurement of growth kinetics, comp = Stern−Volmer competitive analysis. [b] Goodness-of-fit parameter. [c] Measured by LFP in acetonitrile (ACN), this study. [d] Measured in aqueous solution by LFP and/or pulse radiolysis. [e] Reference 30a. [f] Reference 30b. [g] Reference 30c.

of the absolute rate constants of hydroxyl radical toward naphthalene and benzene increases dramatically on changing the solvent from water to acetonitrile, consistent with the reactivity−selectivity principle.[32] To test the veracity of this unexpected result, we sought to independently measure this ratio by analysis of the mixture of products formed upon photolysis (365 nm) of *N*-hydroxypyridine-2-thione (**1**) in acetonitrile containing benzene and naphthalene. Twenty-two measurements were made by gas chromatography using three different ratios of the aromatic reagents at concentrations comparable to those used in the LFP experiments. By GC product studies, the ratio of $k_{benzene}$ to $k_{naphthalene}$ obtained at ambient temperature was 0.069 ± 0.028. The large standard deviation is due to the low absolute yields of phenol and of the 1- and 2-naphthol adducts. This result is in excellent agreement with the same ratio of rate constants (0.052) as that determined by the LFP approach.

We also photolyzed *N*-hydroxypyridine-2-thione (**1**) in neat benzene containing naphthalene. Under these conditions, the absolute yields of phenol and the mixture of naphthols were increased by a factor of at least ten. This led to a ratio of rate constants of 0.16 ± 0.024 in this nonpolar organic solvent mixture, and the ratio was obtained with greater reproducibility than in acetonitrile. In contrast, the ratio of $k_{benzene}$ to $k_{naphthalene}$ in water is 0.83.[30] The GC study confirms that this ratio changes dramatically in organic solvents.

Thus, our experiments, using different techniques, demonstrate that hydroxyl radical reacts faster in water than in acetonitrile. To understand the origin of this effect, high-level theoretical calculations were performed to shed light upon this unexpected result. There have been a number of high-quality computational studies in the literature on hydroxyl radical reactions with benzene and other aromatic hydrocarbons.[33] In these studies, it was concluded that the dominant reaction pathway of hydroxyl radical with these aromatic hydrocarbons was by radical addition to the ring carbons. In some recent reports by Nicolaescu et al. on the reactivity of hydroxyl radical with quinoline,[34] experimental and computational studies showed that the hydroxyl radical addition pathway to the ring carbons was facile and proceeded with small or negligible activation barriers. Furthermore, Nicolaescu et al. demonstrated that the activation barriers were also decreased with computational (dielectric field as well as explicit) models for aqueous solvation.[34b] We will consider similar approaches in the next section to rationalize the unexpected rate enhancement for hydroxyl radical reaction in water relative to that in acetonitrile.

Computational Results

I. Solvent−Hydroxyl Radical Complexes. Two different geometries were located for the complexes between hydroxyl

(32) March, J. *Advanced Organic Chemistry*; John Wiley and Sons: New York, 1985; pp 174−175 and references therein.

(33) (a) Lay, T. H.; Bozzelli, J. W.; Seinfeld, J. H. *J. Phys. Chem.* **1996**, *100*, 6543−6554. (b) Andino, J. M.; Smith, J. N.; Flagan, R. C.; Goddard, W. A., III; Seinfeld, J. H. *J. Phys. Chem.* **1996**, *100*, 10967−10980. (c) Ghigo, G.; Tonachini, G. *J. Am. Chem. Soc.* **1998**, *120*, 6753−6757. (d) Lundqvist, M. J.; Eriksson, L. A. *J. Phys. Chem. B* **2000**, *104*, 848−855. (e) Vivekananda, S.; Wolken, J. K.; Tureček, F. *J. Phys. Chem. A* **2001**, *105*, 9130−9141. (f) Volkamer, R.; Platt, U.; Wirtz, K. *J. Phys. Chem. A* **2001**, *105*, 7865−7874. (g) Tokmakov, I. V.; Lin, M. C. *J. Phys. Chem. A* **2002**, *106*, 11309−11326. (h) Motta, F.; Ghigo, G.; Tonachini, G. *J. Phys. Chem. A* **2002**, *106*, 4411−4422. (i) Johnson, D.; Raoult, S.; Rayez, M.-T.; Rayez, J.-C.; Lesclaux, R. *Phys. Chem. Chem. Phys.* **2002**, *4*, 4678−4686.

(34) (a) Nicolaescu, A. R.; Wiest, O.; Kamat, P. V. *J. Phys. Chem. A* **2005**, *109*, 2822−2828. (b) Nicolaescu, A. R.; Wiest, O.; Kamat, P. V. *J. Phys. Chem. A* **2005**, *109*, 2829−2835.

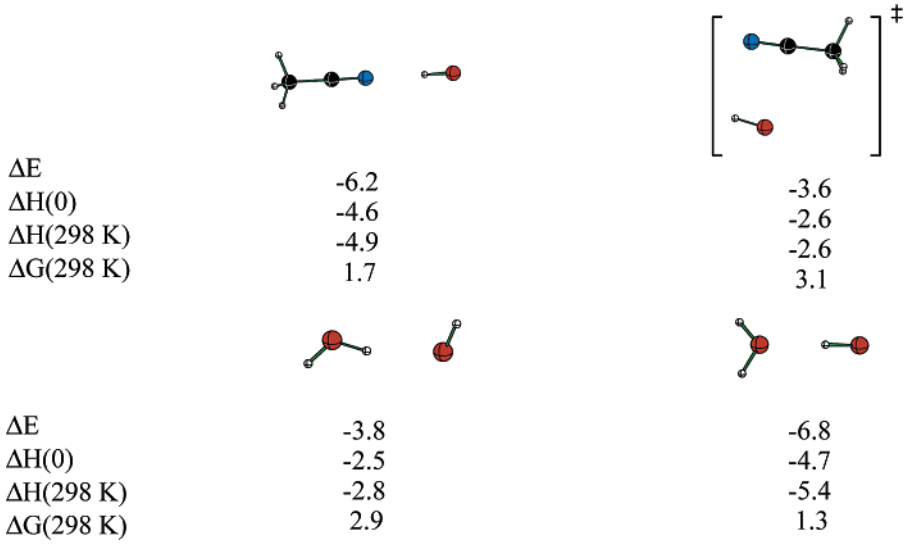

Figure 7. Hydroxyl radical−solvent complexes at the B3LYP/6-311+G**//B3LYP/6-31+G** level (kcal/mol). All energies are relative to the infinitely separated species at the same level of theory.

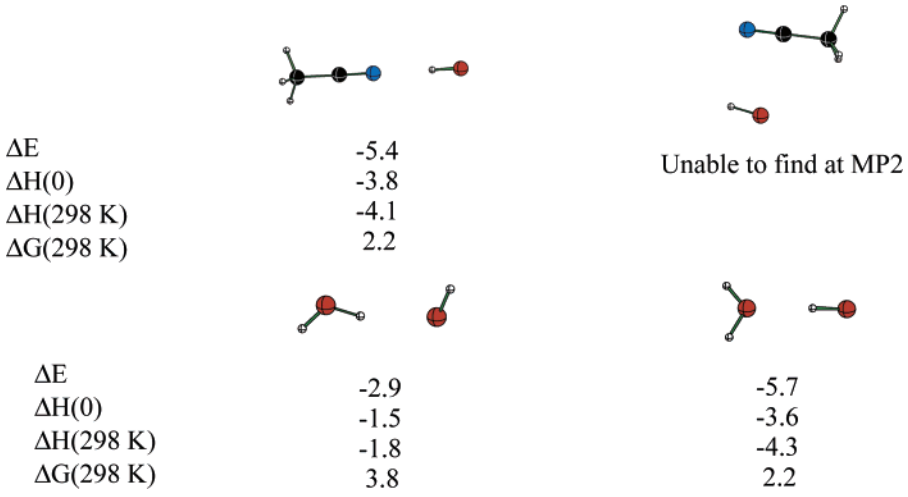

Figure 8. Hydroxyl radical−solvent complexes at the MP2/6-311+G**//MP2/6-31+G** level (kcal/mol). All energies are relative to the infinitely separated species at the same level of theory.

radical with water at the B3LYP/6-311+G**//B3LYP/6-31+G** level of theory. Only one geometry was located for the complex of hydroxyl radical with acetonitrile, and the other structure was a transition state. The results of these calculations are summarized in Figure 7. Energies are presented as relative to the infinitely separated species (as zero).

From this information, it is clear that the most favorably bound complex is one between hydroxyl radical and water. In this complex, the proton of hydroxyl radical is hydrogen bonded to the oxygen of water. This result is in accord with recent experimental[35] and previous computational[36] studies on hydroxyl radical−water complexes. In fact, the recent gas-phase microwave studies of the $(H_2O)HO$ complex suggest that there is a "substantial effect on the electron distribution of the radical upon complexation"[35c] by water and that the most accurate representation is $H_2O^{\delta+}-HO^{\delta-}$.[35d] For hydroxyl radical coordinated with acetonitrile, a similar orientation with a favorable interaction between the hydroxyl radical's proton and the nitrogen of acetonitrile is the lower-energy geometry for the complex between those molecules. The difference in free energy between these lowest-energy geometries is approximately 0.4 kcal/mol in favor of the hydroxyl−water complex.

The same calculations were performed at the MP2/6-311+G**//MP2/6-31+G** level of theory to determine the validity of the density functional theory results. All of the complexes located at the B3LYP/6-31+G** level of theory were again located at the MP2/6-31+G** level. The results of these calculations are summarized in Figure 8. According to the MP2 level of theory, there is very little difference in energy between the water and acetonitrile complexes. It appears that overall, the water complex is very slightly lower in energy, but the difference in free energy is within 0.05 kcal/mol.

(35) (a) Langford, V. S.; McKinley, A. J.; Quickenden, T. I. *J. Am. Chem. Soc.* **2000**, *122*, 12859−12863. (b) Cooper, P. D.; Kjaergaard, H. G.; Langford, V. S.; McKinley, A. J.; Quickenden, T. I.; Schofield, D. P. *J. Am. Chem. Soc.* **2003**, *125*, 6048−6049. (c) Brauer, C. S.; Sedo, G.; Grumstrup, E. M.; Leopold, K. R.; Marshall, M. D.; Leung, H. O. *Chem. Phys. Lett.* **2005**, *401*, 420−425. (d) Ohshima, Y.; Sato, K.; Sumiyoshi, Y.; Endo, Y. *J. Am. Chem. Soc.* **2005**, *127*, 1108−1109. (e) Aloisio, S.; Francisco, J. S. *Acc. Chem. Res.* **2000**, *33*, 825−830.

(36) (a) Kim, K. S.; Kim, H. S.; Jang, J. H.; Kim, H. S.; Mhin, B.-J.; Xie, Y.; Schaefer, H. F., III. *J. Chem. Phys.* **1991**, *94*, 2057−2062. (b) Nanayakkara, A. A.; Balint-Kurti, G. G.; Williams, I. H. *J. Phys. Chem.* **1992**, *96*, 3662−3669. (c) Xie, Y.; Schaefer, H. F., III. *J. Chem. Phys.* **1993**, *98*, 8829−8834. (d) Wang, B.; Hou, H.; Gu, Y. *Chem. Phys. Lett.* **1999**, *303*, 96−100.

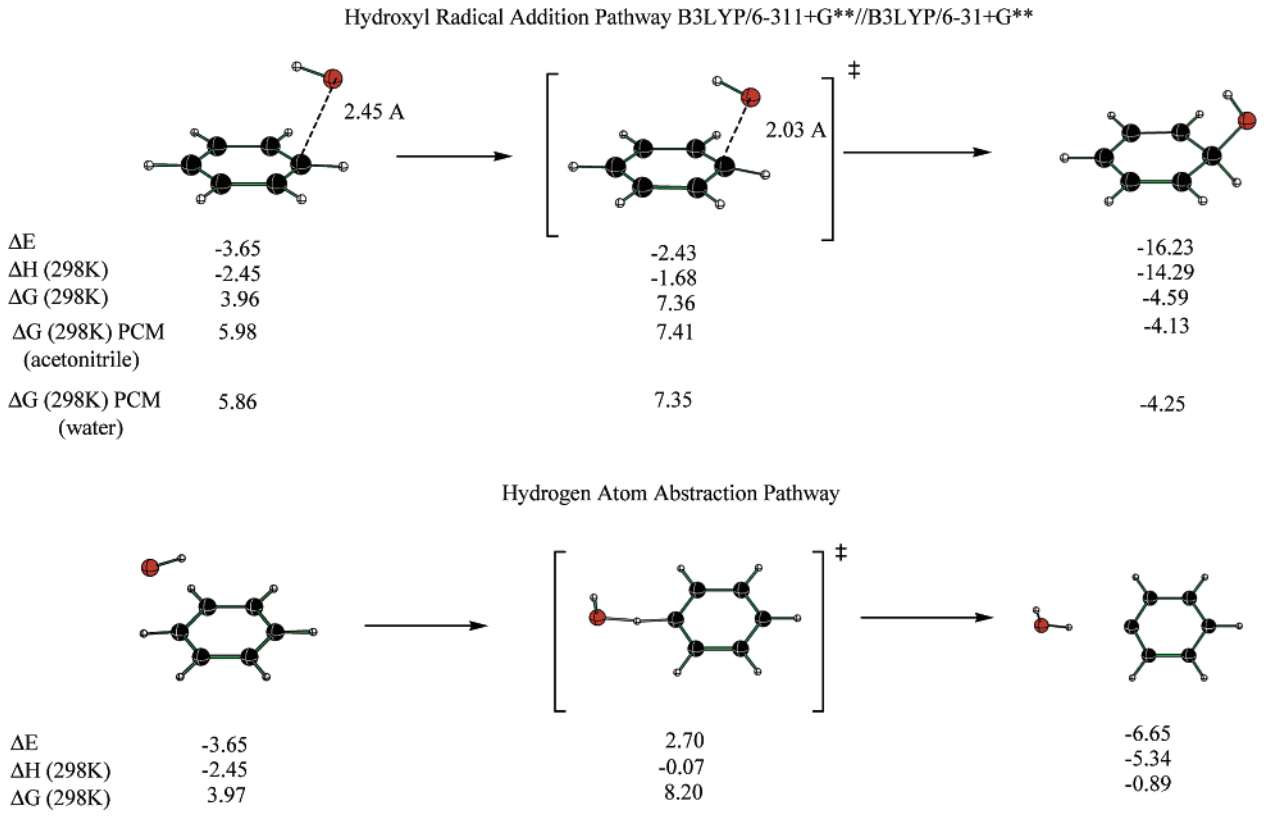

Figure 9. Hydroxyl-radical addition and hydrogen-atom abstraction pathways at the B3LYP/6-311+G**//B3LYP/6-31+G** level of theory (kcal/mol). All energies are relative to the infinitely separated species at the same level of theory.

From the data collected here, it is apparent that an extremely stable complex between the solvent and hydroxyl radical is not the origin of the observed differences in reactivity. In fact, these data seem to suggest that the complex between hydroxyl radical and water would be more stable. Thus, one might expect that the complex of hydroxyl radical with water would have a higher activation barrier due to the subsequent dissociation process and consequentially a slower rate. This observation is contrary to the experimental results, and therefore, pre-reactive complexes cannot be the origin of the enhanced reactivity of hydroxyl radical with benzene in water.

II. Standard Hydroxyl-Radical Addition and Hydrogen-Atom Abstraction Reactions. Calculations were performed at the B3LYP/6-311+G**//B3LYP/6-31+G** level of theory to determine the energetics for the hydroxyl-radical addition and hydrogen-atom abstraction pathways for reaction with benzene. It was important to determine which pathway would be most favorable and if one would, in fact, dominate. To this end, transition states for each pathway were located and then connected to their respective reactants and products. The results of these calculations are summarized in Figure 9. The energies presented are relative to the infinitely separated reactants.

It is apparent from these data that the addition pathway will be the dominant pathway for the reaction between hydroxyl radical and benzene. The free energy of activation for the hydrogen-atom abstraction pathway is nearly 1 kcal/mol higher than that of the addition pathway. The addition pathway should therefore be the predominant reaction between hydroxyl radical and benzene.

To probe the effect of dielectric field on the hydroxyl-radical addition reaction, transition states were located using the polarizable continuum model at the B3LYP/6-311+G**//B3LYP/6-31+G** level of theory under the influence of the dielectric constants of water and acetonitrile. Reactant complexes and products were then located from these transition states. The results of these calculations are given in Figure 9. It is readily apparent from these data that the dielectric field alone (as calculated by PCM) predicts only a 0.06 kcal/mol preference for reaction in water as opposed to that in acetonitrile. This difference is not sufficient to explain the experimental difference in reaction rates.

III. Reactions of Hydroxyl Radical Complexed With One Molecule of Solvent. To probe the effect of specific interactions of solvent molecules on the reaction of hydroxyl radical with benzene, systems were modeled in which one molecule of solvent was complexed with the hydroxyl radical, and transition states were located for the reactions of these complexes with benzene. Two different transition-state geometries were located for each of the complexes between the solvent molecule and hydroxyl radical for the addition reaction. Calculations were first performed at the B3LYP/6-311+G**//B3LYP/6-31+G** level of theory. Calculations were also performed on these reactions at the CBS-QB3 level of theory to attain a more accurate prediction of the relative energies between these systems. The results for the acetonitrile complexes are summarized in Figure 10.

The lowest-energy process for hydroxyl radical complexed with acetonitrile is the pathway in which there is a favorable interaction between a hydrogen of acetonitrile and the oxygen of hydroxyl radical. It should be noted that the complex in which the hydrogen of hydroxyl radical interacts with the electronegative nitrogen of acetonitrile is the more stable pre-

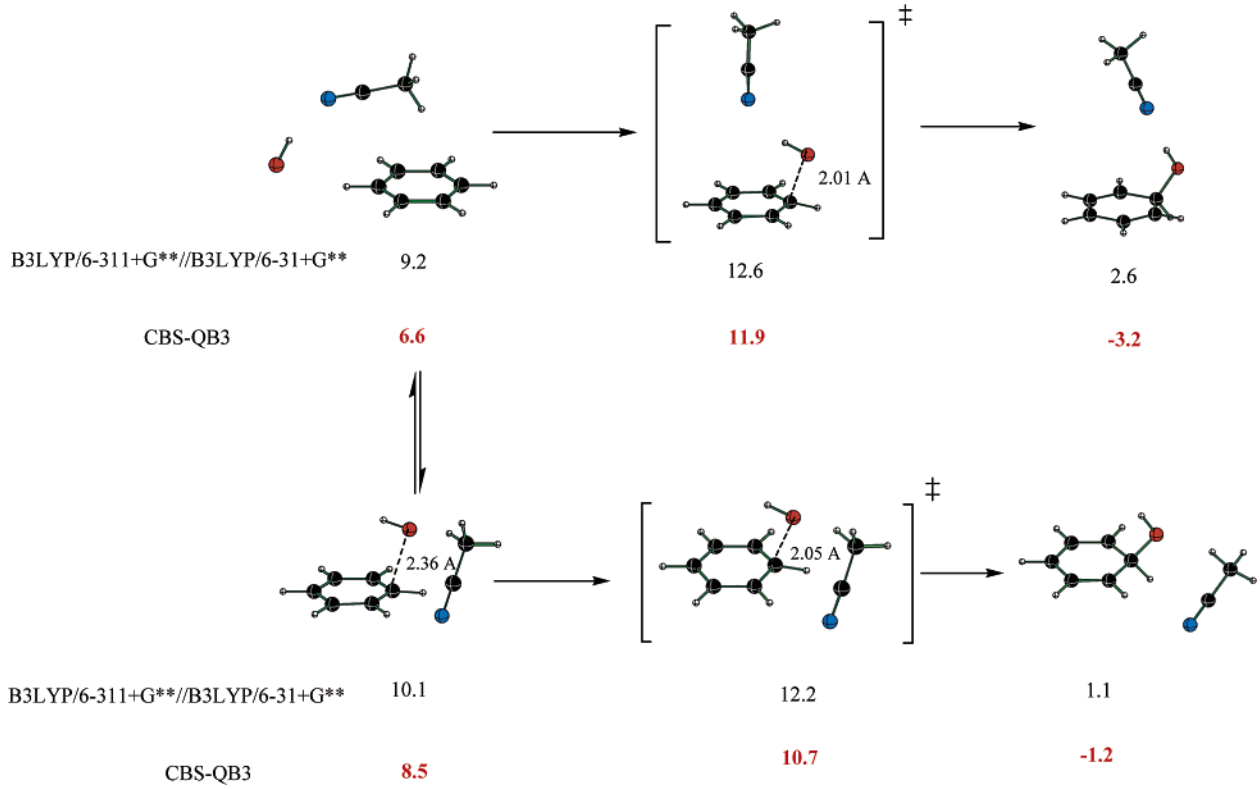

Figure 10. Free energy ΔG (298 K) (kcal/mol) diagram of the reactant complexes (left), transition states (center), and product complexes (right) for the reaction of hydroxyl radical and one acetonitrile molecule with benzene at the B3LYP/6-311+G**//B3LYP/6-31+G** and CBS-QB3 levels in the gas phase. All energies are relative to the infinitely separated species at the same level of theory.

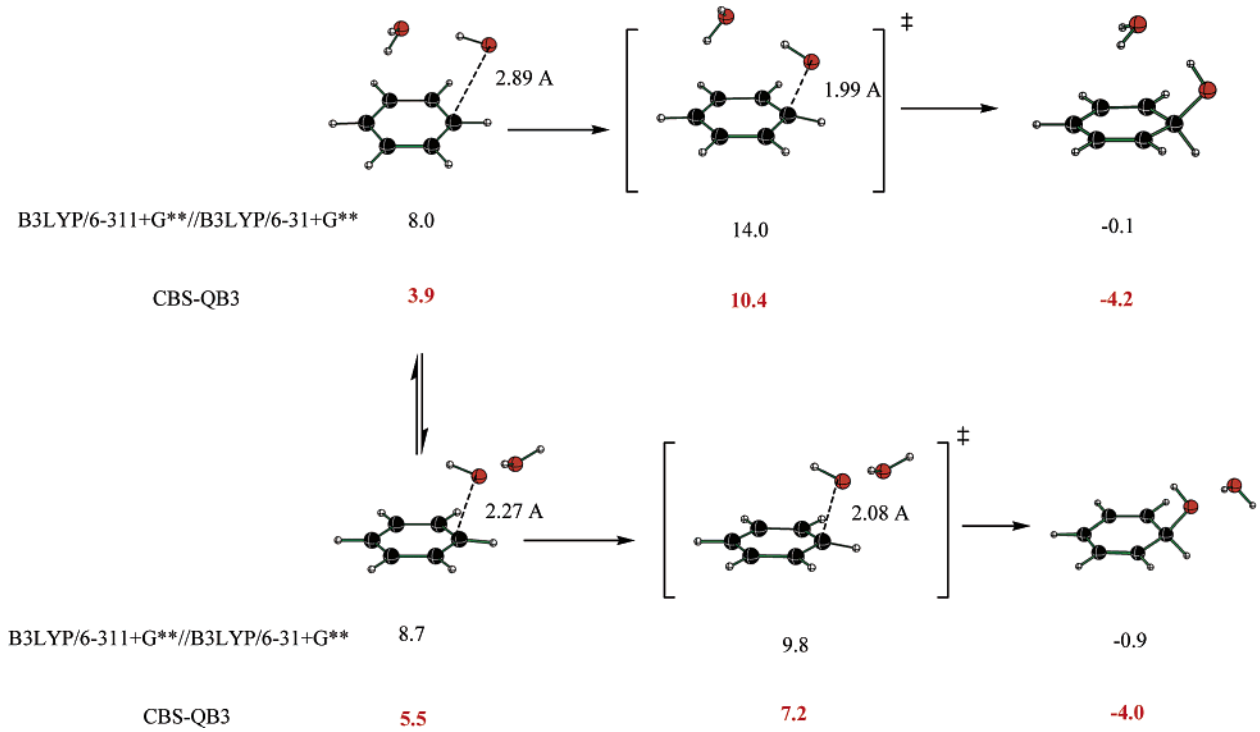

Figure 11. Free energy ΔG (298 K) (kcal/mol) diagram of the reactant complex (left), transition state (center), and product complexes (right) for the reaction of hydroxyl radical and one water molecule with benzene at the B3LYP/6-311+G**//B3LYP/6-31+G** and CBS-QB3 levels in the gas phase. All energies are relative to the infinitely separated species at the same level of theory.

reacting complex, but upon going to the transition state, this orientation is less stable. The lower-energy transition state, albeit by a small margin, has acetonitrile acting as a hydrogen-bond donor.

The results for the water complex reactions are summarized in Figure 11. A similar trend is observed here as was seen in the case of the acetonitrile complex reactions. The reactant complex in which the hydroxyl radical's hydrogen interacts with

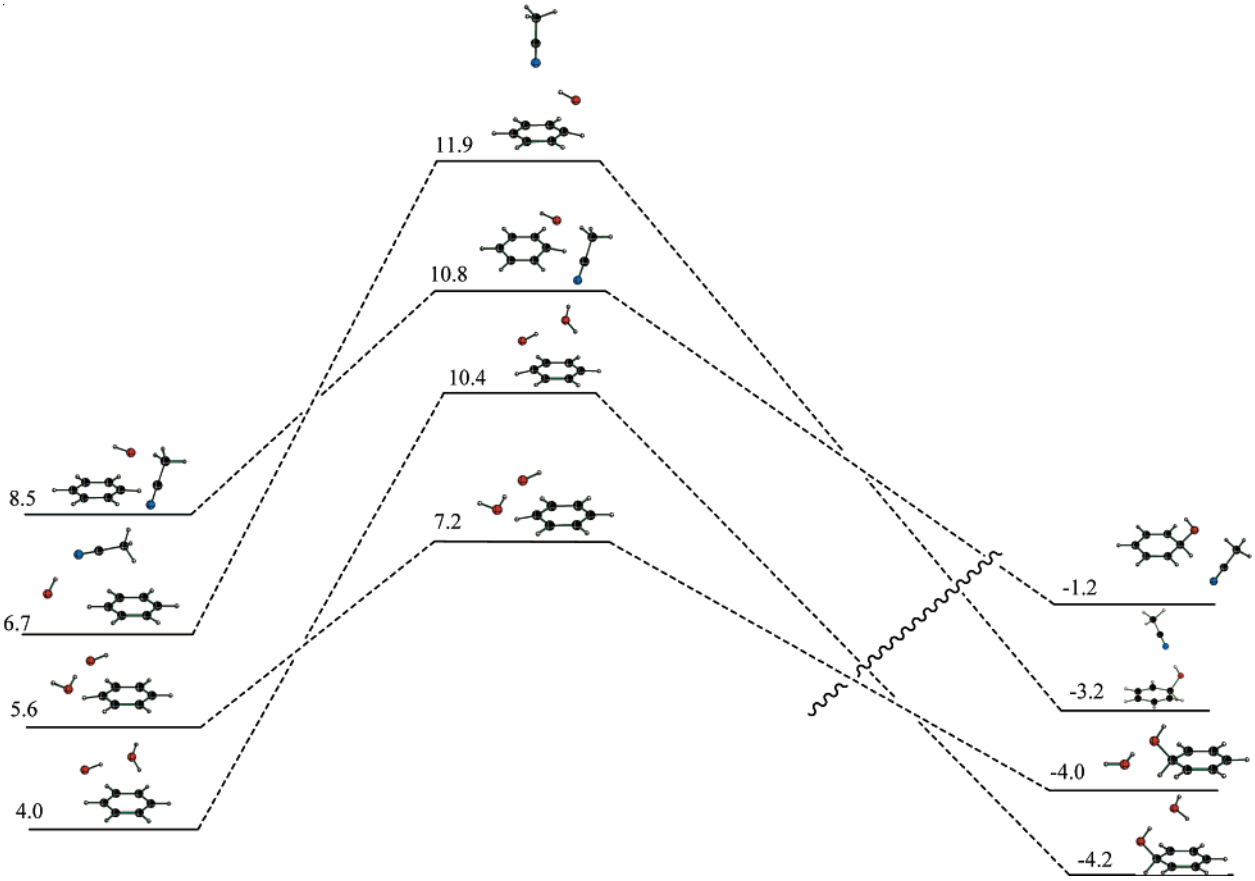

Figure 12. Comparison of gas-phase ΔG (298 K) values for hydroxyl radical complexed to one molecule of solvent in addition reactions with benzene (kcal/mol) at the CBS-QB3 level of theory. All energies are relative to the infinitely separated species at the same level of theory.

Table 3. Comparison of Rates and Activation Barriers for the Reaction of Hydroxyl Radical Complexed with One Molecule of Solvent[a]

	B3LYP/6-311+G**//B3LYP/6-31+G**		CBS-QB3	
solvent	$\Delta G^{\ddagger}$ (kcal/mol)	reaction rate[b] (cm^3 $molecule^{-1}$ s^{-1})	$\Delta G^{\ddagger}$ (kcal/mol)	reaction rate[b] (cm^3 $molecule^{-1}$ s^{-1})
water	9.8	1.61×10^{-14}	7.2	1.42×10^{-12}
acetonitrile	12.2	3.02×10^{-16}	10.7	3.51×10^{-15}
relative value	2.4	53:1	3.5	406:1

[a] Using the lowest-energetic barrier process for each solvent system. [b] Using conventional transition-state theory with a Wigner tunneling correction.

the electronegative oxygen of water is more stable than the complex in which the hydrogen of water interacts with the hydroxyl radical's oxygen. Upon going to the transition state, however, the relative energetics are reversed. This seems to indicate that the most favorable complex for reaction in water is that in which the water acts as a hydrogen-bond donor to the hydroxyl radical moiety.

A comparison of all of the data for the different complexes evolving to the unique transition states is shown in Figure 12. This comparison very clearly demonstrates that the reaction of hydroxyl radical complexed with water has a significantly lower activation barrier than that of the hydroxyl radical−acetonitrile complex. On the basis of these activation barriers, second-order rate constants were calculated for these reactions. A comparison of these rate constants for each reaction is provided in Table 3. According to the B3LYP calculations, the rate of reaction of hydroxyl radical addition to benzene will be approximately 50 times faster in water than in acetonitrile. CBS-QB3 calculations predict, according to this model with only one specific interaction with a solvent molecule, that the reaction will proceed approximately 400 times faster in water than in acetonitrile. Both of these values are in fairly good agreement with the experimentally determined relative rates of approximately 65 to 1.

To verify that, in fact, the addition pathway would be the most dominant pathway, calculations were also performed at the B3LYP/6-311+G**//B3LYP/6-31+G** level of theory for the hydrogen-atom abstraction reaction. The results of these calculations are given in Figure 13. It was only possible to locate one complex between hydroxyl radical and the solvent molecule in each case. It is readily apparent from these results that the activation barrier for this pathway has a larger free energy of activation, by approximately 3 kcal/mol. We can therefore rightly conclude that the addition pathway should be the exclusive pathway for the reaction of hydroxyl radical with benzene at 298 K. It can also be observed from the data in Figure 13 that the complex with water still has a lower activation barrier than the complex with acetonitrile. This may indicate that the same stabilization factor that is operative in the addition process may also be at work in the abstraction process.

To obtain some idea of the effect of both the specific solvent interactions as well as that of a solvent's dielectric field, single-point energy calculations were performed on the gas-phase stationary points as well as with the infinitely separated reactants for the addition process under the polarizable continuum model (PCM) with the B3LYP/6-311+G**//B3LYP/6-31+G** level of theory. This provides us with a bottom-of-the-well energy

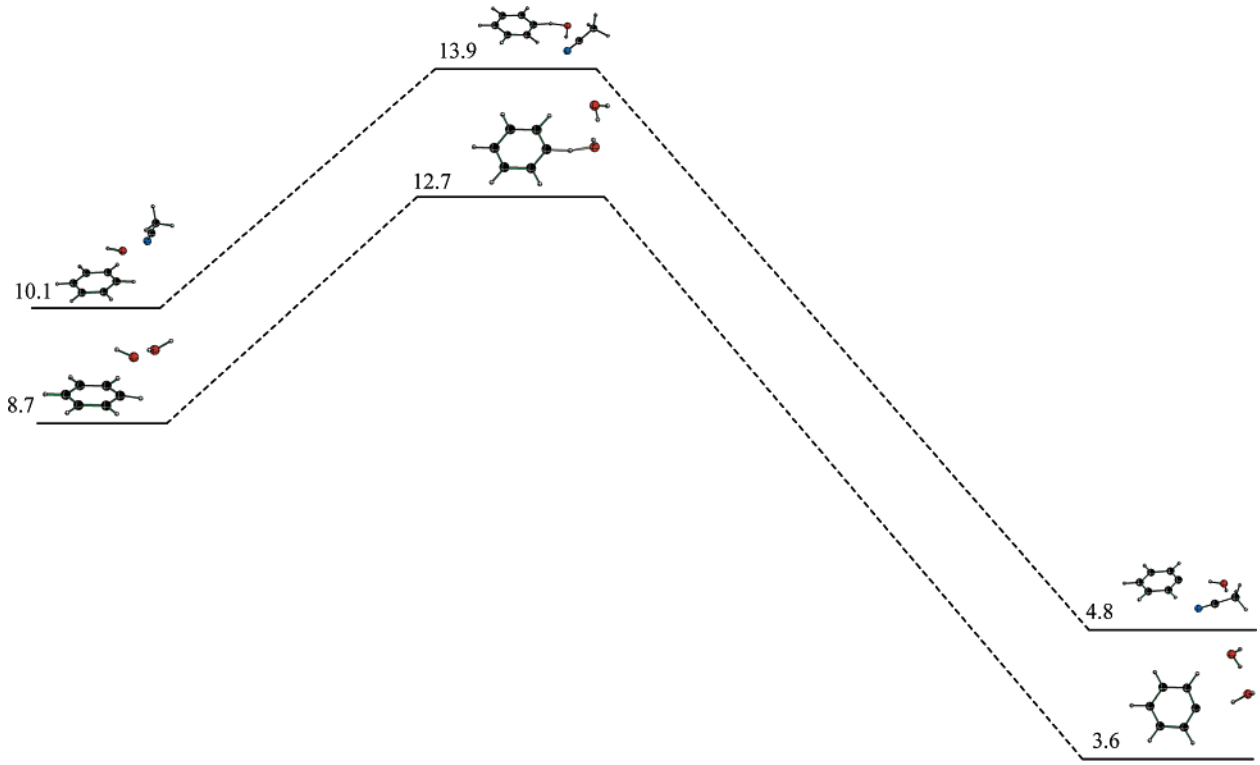

Figure 13. Comparison of ΔG (298 K) values for hydroxyl radical complexed to one molecule of solvent in hydrogen-atom abstraction reactions with benzene (kcal/mol) at the CBS-QB3 level of theory in the gas phase. All energies are relative to the infinitely separated species at the same level of theory.

with the PCM solvation model. The results of these calculations are provided in Figure 14. From this figure, it is apparent that the relative energy between the transition states in different solvents ($\delta\Delta E = 2.9$ kcal/mol) is approximately the same as those of the gas-phase calculations ($\delta\Delta E = 2.4$ kcal/mol). It appears that the bulk dielectric effect does not significantly affect the rate enhancement observed in water as opposed to that in acetonitrile. The specific interaction of at least one molecule of solvent appears to be the predominant cause of the differences in rate observed between the two solvent systems. The PCM single-point energy calculations do change the relative energetics of the reactants and products slightly, but this is a small perturbation compared to the observed difference in rates.

IV. Reactions of Hydroxyl Radical Complexed With Two Molecules of Solvent. To further probe the effect of solvent on the reaction of hydroxyl radical with benzene, we examined the reaction of hydroxyl radical with benzene in the presence of two explicit solvent molecules. To determine the placement of the solvent molecules, a Monte Carlo search protocol followed by minimization under the MM3 force field was performed on **2**. This molecule is believed to provide a suitable initial model for the transition state of hydroxyl-radical addition to benzene. The three lowest-energy, unique geometries obtained from this search with acetonitrile and water were then modified to create suitable transition states for the reaction and used as the guess geometries for the transition state at the B3LYP/6-31+G** level of theory. All structures returned the exact same geometry for the transition state with the respective solvent molecules. The reactants and products were determined by displacement along the normal coordinate for the vibrational frequency. The Monte Carlo search coupled with the MM3 force field was not, however, able to predict a low-energy conformation in which the hydrogen of the hydroxyl group would lie directly over the ring. This most likely is a limitation of the MM3 force field. To ensure that this conformation was probed, the transition states obtained were modified (maintaining the appropriate interactions with the solvent molecules). Transition states were located in this fashion and were, in fact, calculated to be lower in energy than those found initially. Reactants and products were then located for these transition states as well. The lowest-energy pathways for acetonitrile and water are shown in Figure 15, and a complete comparison of all of the transition states located with two molecules of solvent is shown in Figure 16. Rate constants were then calculated for each of the pathways, and the data are summarized in Table 4. By including two solvent molecules, the rate of reaction in water is enhanced by approximately 200 times over the rate in acetonitrile according to the B3LYP calculations. The activation barrier for hydroxyl-radical addition to benzene is 3.2 kcal/mol lower in water than in acetonitrile. These results are again in very good agreement with the experimental observations for these systems.

Similar calculations were then performed on a system that included one molecule of water and one of acetonitrile. Using the same Monte Carlo search and modification process described above, it was possible to locate one transition state at the B3LYP/6-311+G**//B3LYP/6-31+G** level of theory for addition of hydroxyl radical to benzene. The transition state located was one in which the acetonitrile acted as a hydrogen-bond donor with hydroxyl radical and the water molecule acted as a hydrogen-bond acceptor with hydroxyl radical. Due to previous calculations, it was believed that a second transition state in which the donor and acceptor molecules were switched should be possible. To this end, the positions of the water and acetonitrile molecules were manually exchanged, and a transition state was then located for this system. Both of the transition states located were those in which the hydrogen of hydroxyl

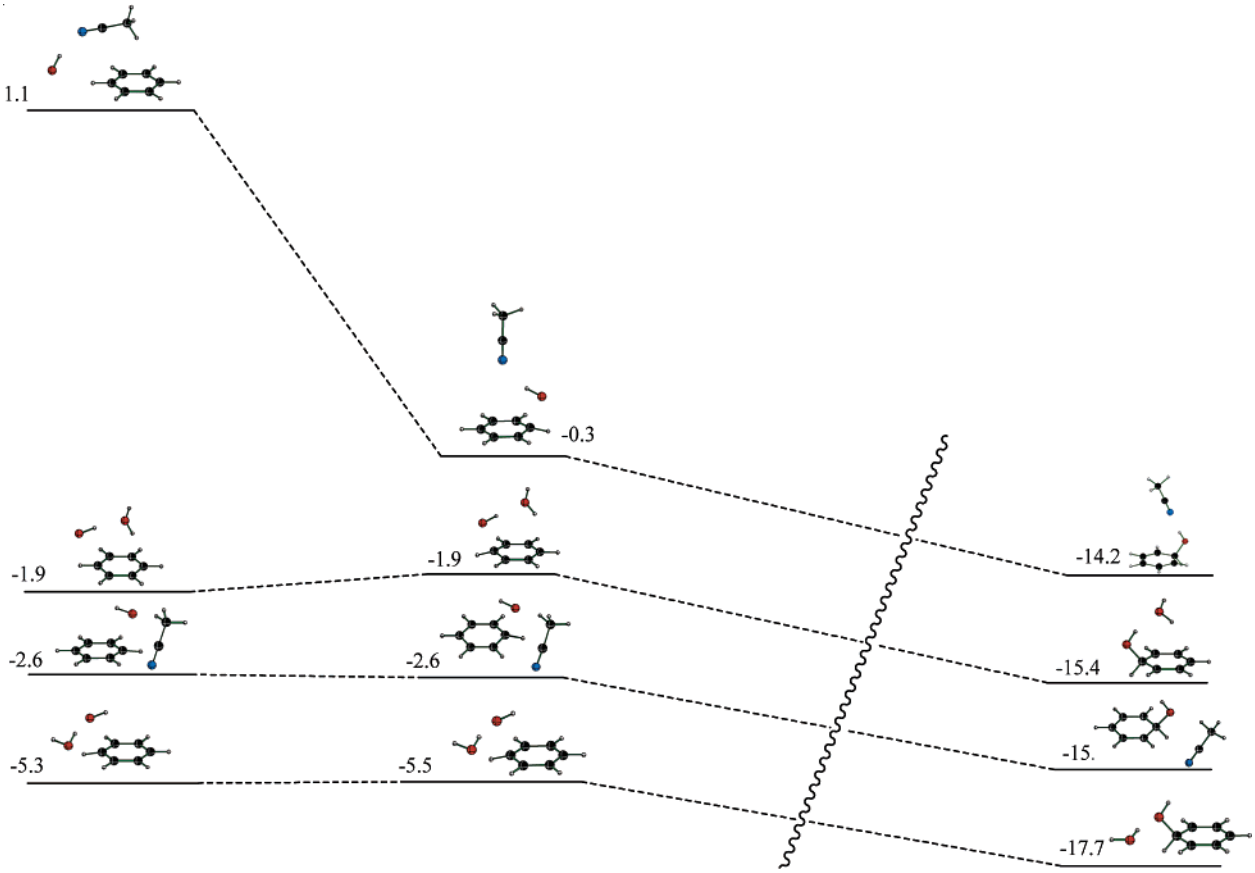

Figure 14. Comparison of ΔE (bottom-of-the-well) values for hydroxyl radical complexed to one molecule of solvent in addition reactions with benzene (kcal/mol) at the PCM B3LYP/6-311+G**//B3LYP/6-31+G** level appropriate for each solvent. All energies are relative to the infinitely separated species at the same level of theory.

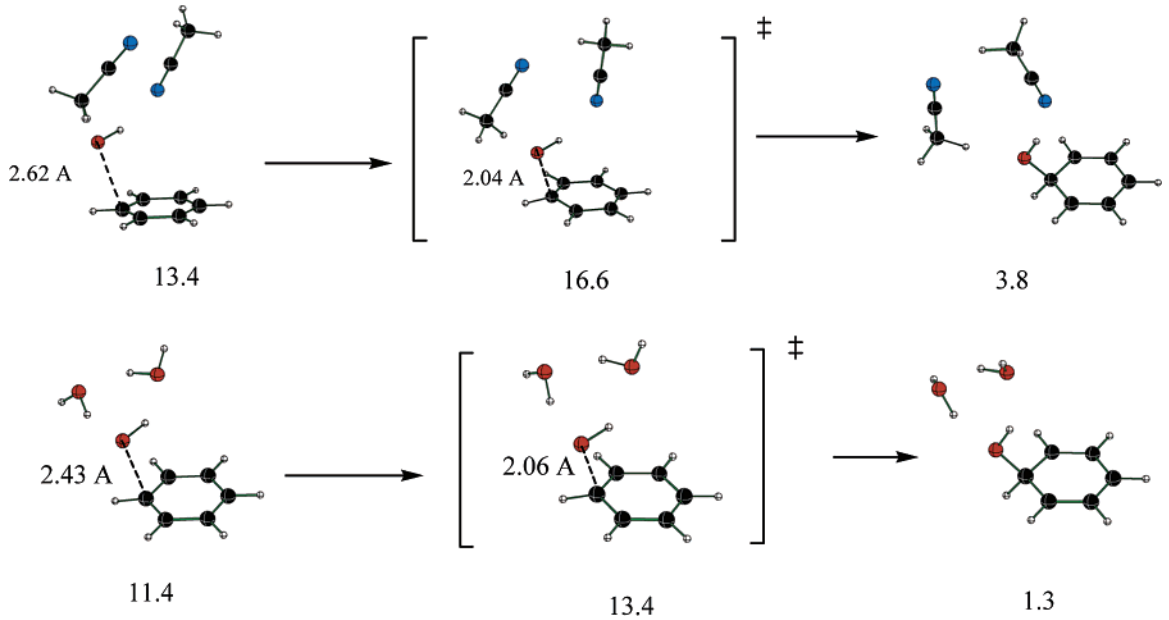

Figure 15. Free energy ΔG (298 K) (kcal/mol) diagram of the reactant complexes (left), transition states (center), and product complexes (right) for the reaction of hydroxyl radical and two molecules of solvent with benzene at the B3LYP/6-311+G**//B3LYP/6-31+G** level of theory in the gas phase. All energies are relative to the infinitely separated species at the same level of theory.

radical was pointed outside of the ring so then searches were also performed to locate those with the hydrogen over the ring. These were located and found to be the lowest-energy transition states. The results for the lowest-energy transition states are shown in Figure 17.

These results illustrate some very interesting points. The pre-reacting complex wherein acetonitrile acts as the hydrogen-bond donor is actually lower in energy than that in which water acts as the hydrogen-bond donor. It is only upon evolving into the transition state that this is reversed. This would appear to

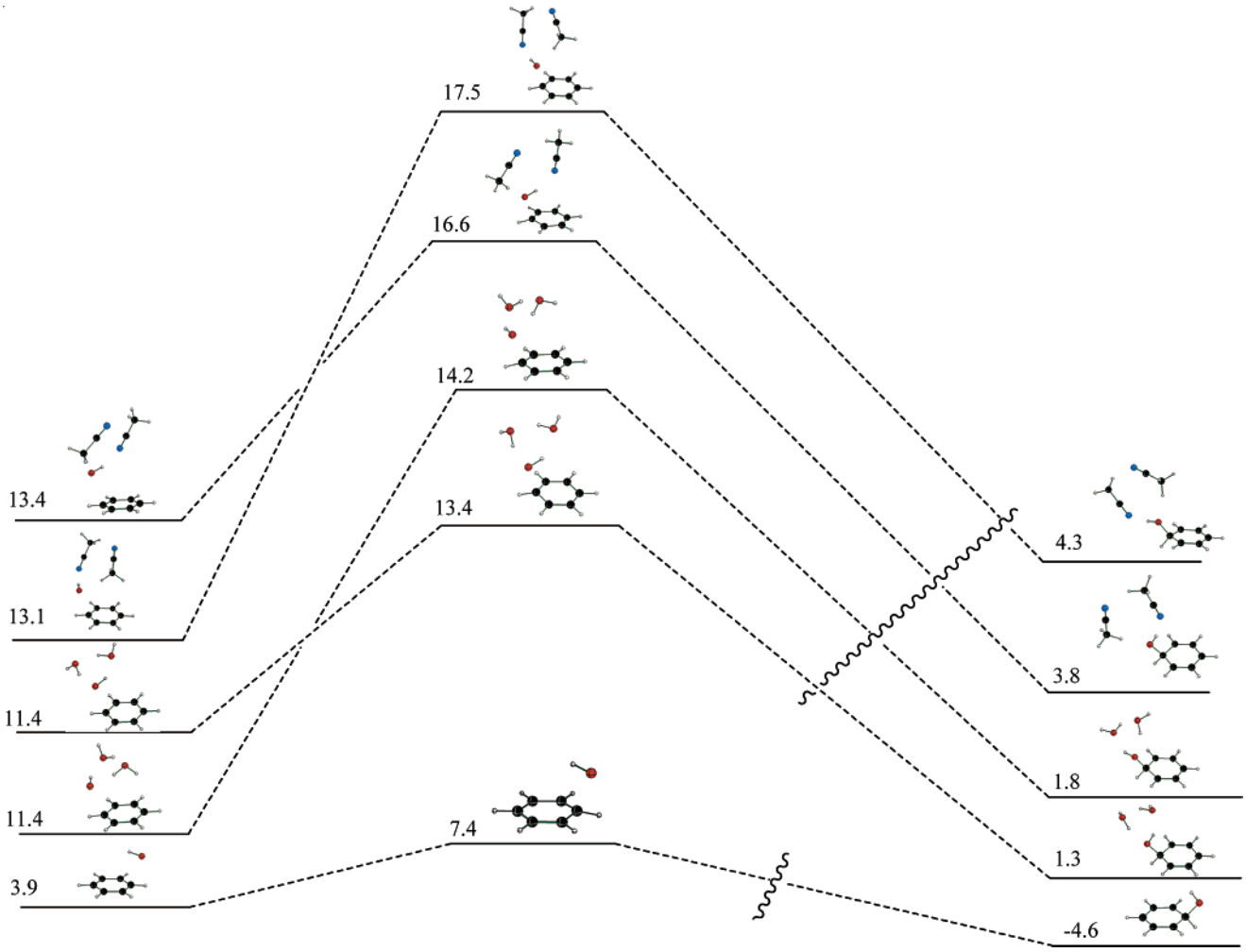

Figure 16. Comparison of ΔG (298 K) values for hydroxyl radical complexed to two molecules of solvent in addition reactions with benzene (kcal/mol) at the B3LYP/6-311+G**//B3LYP/6-31+G** level of theory. All energies are relative to the infinitely separated species at the same level of theory.

Table 4. Comparison of Rates and Activation Barriers for the Reaction of Hydroxyl Radical Complexed with Two Molecules of Solvent[a]

	B3LYP/6-311+G**//B3LYP/6-31+G**	
solvent	$\Delta G^{\ddagger}$ (kcal/mol)	reaction rate[b] (cm^3 $molecule^{-1}$ s^{-1})
water	13.4	1.65×10^{-19}
acetonitrile	16.6	3.66×10^{-17}
relative value	3.2	221:1

[a] Using the lowest-energetic barrier process for each solvent system. [b] Using conventional transition-state theory with a Wigner tunneling correction (see Experimental and Computational Methods section).

indicate very strongly that there is a significant change, upon forming the transition state, in the nature of the hydroxyl radical. It should also be noted that the activation barrier for the lower-energy pathway is very similar to that calculated for the reaction complexes of two water molecules and hydroxyl radical with benzene. The slightly higher activation barrier in the mixed case can be rationalized by the fact that acetonitrile would be expected to act as a poor hydrogen-bond acceptor with hydroxyl radical and as a poorer hydrogen-bond donor to the water molecule. In a solution of 50% acetonitrile and 50% water, we would expect, on the basis of these calculations, that the rate of reaction would be nearly identical to that in water.

V. Natural Population Analysis of Single Solvent Complexes. To determine the origin of the difference in reactivity based upon solvent, a natural population analysis (NPA) was performed on the B3LYP/6-311+G**//B3LYP/6-31+G** stationary points of the reaction of hydroxyl radical complexed with one molecule of solvent and benzene. The NPA data for the lowest-energy transition states for the complexes with water, acetonitrile, and the standard hydroxyl-radical addition are provided in the Supporting Information and tabulated in Table 5.

Several interesting observations can be made. First of all, in all three situations, it is apparent that the charge on hydroxyl radical becomes more negative upon progressing from the pre-reacting complex to the transition state (Table 5). Simultaneously, the charge on benzene becomes more positive. The positive charge appears to be accumulating primarily at the carbons ortho and para to the addition of hydroxyl radical, as one would expect from resonance theory. One can also observe a change in the spin density upon going from the pre-reacting complex to the transition state. The spin density on hydroxyl radical decreases in forming the transition state, and the spin density on benzene increases. These observations indicate that the hydroxyl radical becomes more anionic and looks more like hydroxide anion in the transition state. At the same time,

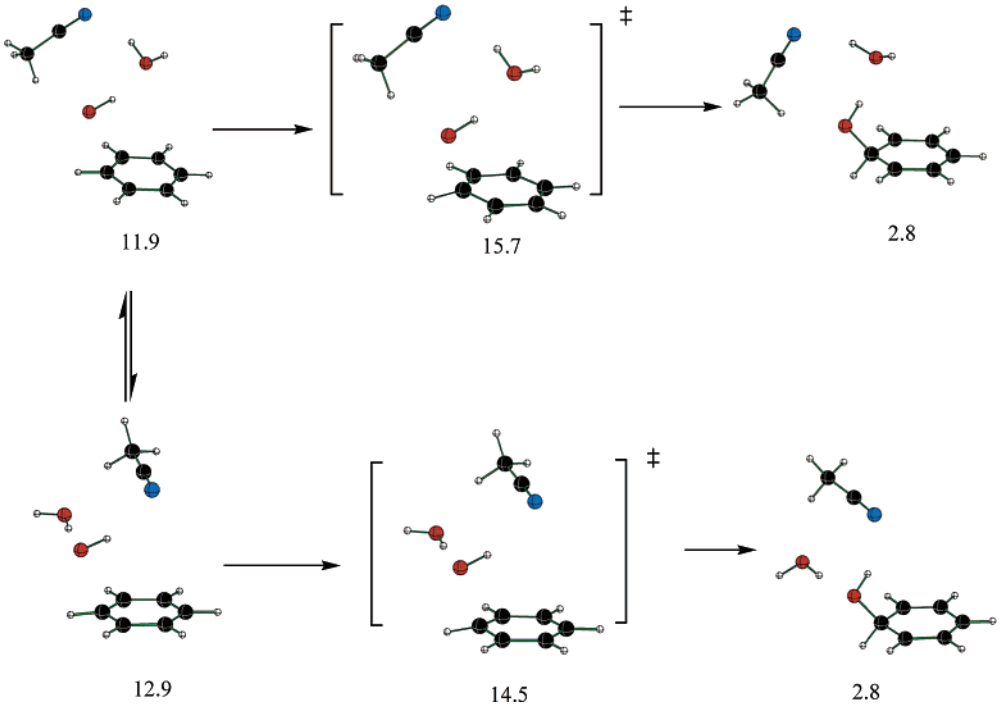

Figure 17. Free energy ΔG (298 K) (kcal/mol) diagram of the reactant complexes (left), transition states (center), and product complexes (right) for the reaction of hydroxyl radical and two molecules of solvent (one molecule each of acetonitrile and water) with benzene at the B3LYP/6-311+G**//B3LYP/6-31+G** level of theory in the gas phase. All energies are relative to the infinitely separated species at the same level of theory.

Table 5. Sum of Charge and Spin Density on Each Moiety Based on NPA Results[a]

		reactant complex			transition state		
solvent		solvent molecule	hydroxyl radical	benzene	solvent molecule	hydroxyl radical	benzene
water	charge	−0.02	−0.20	0.23	−0.02	−0.26	0.28
	spin density	0.00	0.72	0.28	0.00	0.61	0.39
acetonitrile	charge	0.00	−0.17	0.18	0.00	−0.26	0.26
	spin density	0.00	0.78	0.22	0.00	0.61	0.39
no solvent	charge	*b*	−0.12	0.12	*b*	−0.23	0.23
	spin density	*b*	0.85	0.15	*b*	0.37	0.37

[a] At the B3LYP/6-311+G**//B3LYP/6-31+G** level of theory. [b] Not applicable.

benzene looks more like the radical cation species in the transition state.

The observations described above lead to the expectation that the ability to stabilize either the developing negative charge on hydroxyl radical or the developing positive charge on the benzene ring should stabilize the transition state. This would lead to a lowering of the activation barrier and perhaps a shift of the transition state to earlier along the reaction coordinate. This is, in fact, what the NPA data reveal. Water acts as a better hydrogen-bond donor than acetonitrile due to the more positive charge of its hydrogens. As such, the water better stabilizes the transition state, and the transition state is formed earlier along the reaction coordinate. This shift of the transition state can be observed based on the length of the C−O bond being formed. This bond length is longer in acetonitrile (2.06 Å) than for the standard, gas-phase addition reaction (2.02 Å) and longer still in water (2.08 Å).

These results are entirely consistent with our previous characterization of the reaction of halogen radicals with benzene.[37] We reported earlier that, in their reactions with benzene, fluorine atom forms only an $\eta_1-\sigma$ complex,[38] in a manner very similar to hydroxyl radical.[11f] Such behavior has been experimentally verified[38,39] and is expected for an attacking moiety that is quite electronegative and can stabilize the incipient negative charge as well as ionize the aromatic ring. However, as the electronegativity of the incoming radical is attenuated, the σ complex becomes disfavored. In fact, chlorine atom forms a loose $\eta_1-\pi$ complex, while Br and I interact with the π system in either loose η_1 or η_6 fashions.

These observations for hydroxyl radical are entirely consistent with the commonly held view of hydroxyl radical as being "electrophilic" when reacting with electron-rich aromatic rings, such as DNA bases, for which the radical cation can be well stabilized by the organic substrate. We have recently reported additional data which support this view for the reactions of hydroxyl radical with other monocyclic and bicyclic aromatic hydrocarbons.[40] Overall, such generation of a hydroxide anion

(37) Tsao, M.-L.; Hadad, C. M.; Platz, M. S. *J. Am. Chem. Soc.* **2003**, *125*, 8390−8399.

(38) The heat of formation of the σ complex is available; see Grover, J. R.; Wen, Y.; Lee, Y. T.; Shobatake, K. *J. Chem. Phys.* **1988**, *89*, 938.

(39) (a) Perry, R. A.; Atkinson, R.; Pitts, J. N., Jr. *J. Phys. Chem.* **1977**, *81*, 296−304. (b) Tully, F. P.; Ravishankara, A. R.; Thompson, R. L.; Nicovich, J. M.; Shah, R. C.; Kreutter, N. M.; Wine, P. H. *J. Phys. Chem.* **1981**, *85*, 2262−2269. (c) Wahner, A.; Zetsch, C. *J. Phys. Chem.* **1983**, *87*, 4945−4951.

moiety in the transition state for hydroxyl-radical addition to benzene completely rationalizes the difference in rate coefficients observed between the reaction in water and in acetonitrile. However, such an electrophilic role of hydroxyl radical will be heavily dependent on the ability of the organic substrate to stabilize the incipient radical cation. DNA bases, due to their electron-rich nature, can favor such radical cations. Other substrates, such as nitrones,[7] may not be able to stabilize such a radical cation, and therefore, hydroxyl radical may appear less electrophilic. Further tests of this hypothesis with other organic substrates are in progress.[40]

(40) Poole, J. S.; Shi, X.; Hadad, C. M.; Platz, M. S. *J. Phys. Chem. A* **2005**, *109*, 2547−2551.

Acknowledgment. Support by the NSF-funded Environmental Molecular Science Institute at the Ohio State University (CHE-0089147) is gratefully acknowledged. We also thank the Ohio Supercomputing Center for generous computational resources.

Supporting Information Available: Additional discussion and validation of the laser flash photolysis methodology, including results obtained with Freon-113 and CCl_4 as solvents. Figures of NPA data, tables of energies, Cartesian coordinates, vibrational frequencies. This material is available free of charge via the Internet at http://pubs.acs.org.

JA043692Q